TECHNISCHE UNIVERSITÄT
CHEMNITZ

Master Thesis

Quantum Dots in Polymer Matrices on Silicon for Photovoltaic Applications

Submitted by
Dipiyanka Shrestha
Matriculation Number: 671200
Advanced Functional Materials

Examiner
Prof. Dr.Dr.h.c. Dietrich R.T. Zahn

Supervised by
Dr. Yevhenii Havryliuk
Dr. Oleksandr Selyshchev

A Master thesis submitted to Technical University of Chemnitz in fulfillment of the requirement for the degree of Masters in Advanced Functional Materials

2024

Declaration

I hereby confirm the following:

• I hereby confirm that the thesis work is original and has not been submitted to any other University or Institution for higher degree purposes.

• I hereby grant the Technical University of Chemnitz the permission to reproduce and distribute publicly paper and electronic copies of this project document in whole or in part in any medium now known or hereafter created in accordance with the Policy on Intellectual Property.

• I have fulfilled all requirements as prescribed by the University and provided 1 copy of my master thesis report in PDF.

Name and signature

Date and Ort:

Abstract

The increasing energy demand leads to increased research and development of alternative energy sources. Together with ecological and economic issues the requirements for new materials used in photovoltaics must be cost-effective, eco-friendly, and possess a direct bandgap to absorb the entire solar spectrum adequately. Cu_2ZnSnS_4 (CZTS) quantum dots (QDs), known for their non-toxic, cheap components and direct bandgap of 1.4–1.7 eV with high absorption ($\sim 10^4$ cm^{-1}) are emerging as promising candidates [1]. This research explores the use of low-temperature colloidal synthesis—a green chemistry approach—to fabricate CZTS QDs [2]. Another widely used material in photovoltaic applications is the p-type conductive polymer PEDOT:PSS. This study integrates CZTS QDs into a conductive PEDOT:PSS matrix. Composite films of CZTS QDs and PEDOT:PSS were prepared in various ratios and spin-coated onto n-type Silicon (Si) substrate, with optimized spinning speed, time, and acceleration [3]. Both thermal annealing and flash lamp annealing (FLA) were employed, and their effects on film properties were compared. Following the annealing process, a gold grid pattern was applied using a thermal evaporator to act as the top electrode, improving electrical connectivity and boosting the performance of the device. Photovoltaic cells are characterized using a solar simulator to test and evaluate the device's performance in a controlled lab setting. [4] Moreover, even at concentrations as low as 4% of CZTS QDs in PEDOT:PSS, enhanced solar cell efficiencies were observed relative to pure PEDOT:PSS. Furthermore, alternative deposition strategies were explored, including single-layered and double-layered deposition of CZTS and PEDOT:PSS. Particularly, when CZTS and PEDOT:PSS were deposited layer by layer, not mixed, and CZTS was applied via spray coating with seven spraying cycles, the efficiency reached its maximum value.

Acknowledgments

I would like to express my sincere gratitude to Prof.Dr.Dr.h.c. Dietrich R. T. Zahn for providing me this opportunity to do master thesis with all the lab facilities.

I am grateful to my supervisors Dr. Yevhenii Havryliuk and Dr. Oleksandr Selyshchev for guiding me through every step of my laboratory work. I appreciate them for their continuous support, constant encouragement, expert advice, motivating recommendations, patience, and desire to convey useful information.

I am immensely thankful to Dr. Narmina Balayeva for her invaluable feedback and thorough review of my report. I would also like to offer my heartful thanks to all of my Semiconductor Physics group colleagues for their continuous encouragement and productive cooperation.

Contents

List of Figures

List of Tables

List of Abbreviations

PV Photovoltaics

CZTS copper zinc tin sulfide

FLA Flash Lamp Annealing

QDs Quantum Dots

OLEDs Organic Light-emitting diodes

P3HT Poly(3-hexylthiophene)

PCE Power Conversion Efficiency

DMSO dimethyl sulfoxide

PEDOT:PSS Poly(3,4-ethylenedioxythiophene) polystyrene sulfonate

EG ethylene glycol

DMF N,N-dimethyl formamide

THF tetrahydrofuran

NCs Nano crystals

PVD Physical Vapor Deposition

JSC short-circuit current

VOC open-circuit voltage

DI Deionized

N-CQDs nitrogen-doped carbon quantum dots

DC Direct Current

RF Radio Frequency

LCD Liquid Crystal Display

TFT Thin-Film Transistor

IC Integrated Circuit

MEMS Micro-Electro-Mechanical Systems

rpm revolutions per minute

IV Current Voltage

Si Silicon

dsp double-side polished

CVD Chemical Vapor Deposition

MAA Mercaptoacetate

SDS Sodium dodecyl sulfate

HF Hydrofluoric acid

FF Fill Factor

1 Introduction

1.1 Advanced Photovoltaic Technology: A Sustainable Future

In the present world, the escalating global population leads to a never-ending demand for energy that impacts every facet of life. The immensity of this energy requirement is undeniable, prompting a critical examination of its sources. Energy resources are commonly divided into renewable and non-renewable types, with the fearful realization that non-renewable sources are finite and will inevitably deplete over time. Considering the approaching shortage, the importance of renewable sources cannot be overstated. Renewable energy is crucial not just for meeting the increasing demand for energy sustainably but also to reduce the detrimental environmental impacts. The principal sources of renewable energy include wind, solar, biomass, geothermal, hydropower, and tidal support. [5]

Photovoltaic (PV) is one of the most potential types of renewable energy, which directly convert solar energy into electricity. The sun, its constant and immense powerhouse, has the potential to supply an enormous portion of our energy requirements. In addition, PV technology is notable for its ecological sustainability, as it produces no noxious byproducts or greenhouse gases during the power-generation process. Increased global consciousness regarding environmental issues and the imperative for sustainable methodologies has contributed to the surge in solar energy's popularity. [6] Solar installations have become increasingly efficient and economical due to continuous technological progress; they can be constructed in any desired scale based on the requirements. The abundance of sunlight provides a reliable and renewable energy source, while government incentives and increased public awareness further enhance the appeal of photovoltaic systems. [7]

PV has a promising future with wide acceptance as the world continues to prioritize sustainable energy solutions. Scientists and Engineers are actively investigating new materials, developing innovative technologies, and increasing the efficiency of solar cells. [8]

1.2 Materials Perspective for Photovoltaic

Materials play an important role in PVs, determining the efficiency and performance of solar cells. The right selection of materials, such as semiconductors, absorbers, and transparent conductive layers, is critical for successfully harnessing and converting sunlight into electrical energy. [9] Ongoing research explores innovative materials like organic polymers and quantum dots to improve the performance of solar cells [10].

To provide efficient energy conversion, materials for PVs should fulfill several requirements. In particular, materials for PV should have a high absorption coefficient, high electron mobility, low recombination rates, a long carrier lifetime, and a band gap that allows sufficient absorption in all solar spectral ranges. [11]

In PV, nanocrystals (NCs) have shown great promise. It can be used to absorb light or to transport charge in PVs. In general, NCs are crystalline particles with at least one dimension less than 100 nm [12]. They have a high surface area to volume ratio due to their small size, which provides them with unique optical, electrical, and catalytic properties that distinguish them from their bulk form. They have several applications, including drug delivery, where they are used as carriers for drugs, proteins and other bioactive molecules in the targeted cells and tissues. It is also used in biomedical imaging, environmental remediation, catalysis, and optoelectronics. [13]

Quantum dots (QDs) are the NCs whose dimension is less than 10 nm. Scientists and Engineers are actively investigating new materials, developing innovative technologies, and increasing the efficiency of solar cells. The electronic and optical characteristics of these NCs are determined by their size and shape.

It has attracted interest as an advantageous material for enhancing the performance of solar cells due to its unique properties such as size-tunable band gap, multiple exciton generation, and electron transport layer, which can reduce recombination losses [15]. Scientists and Engineers are actively investigating new materials, developing innovative technologies, and increasing the efficiency of solar cells as they require low manufacturing energy, a thin layer of absorber material, and the potential to be used on flexible substrates [16].

Another type of material that is promising and widely used for PVs are polymers. Polymers are macromolecules that form by linking one or more types of small chemical units known as monomers. These monomers repeat themselves throughout the structure of the molecule, creating long chains that define the properties of the polymer. [17]

Polymeric materials are scalable, low-cost to manufacture, and inherently flexible, which makes them suitable for solar panels that are both lightweight and versatile.

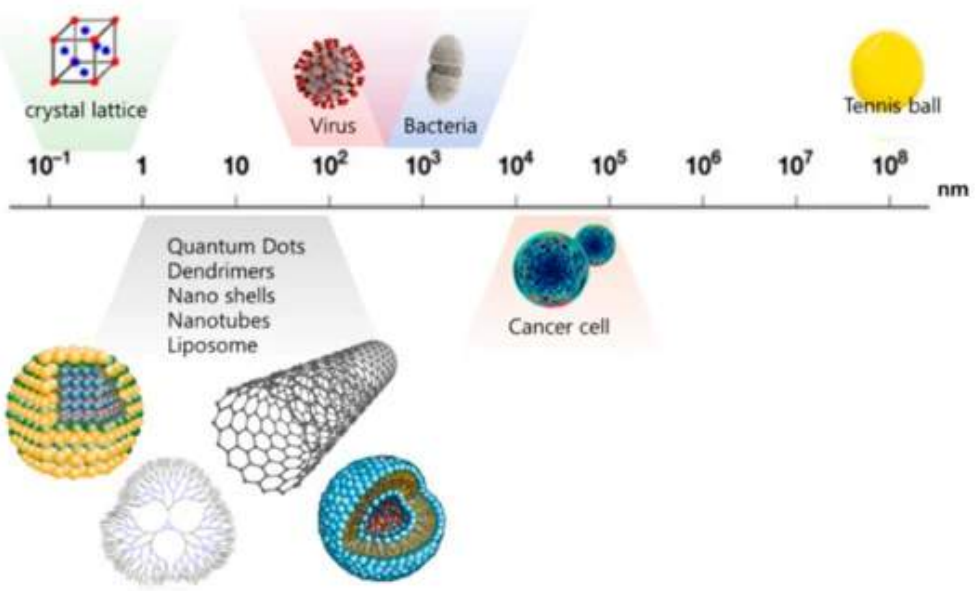

Figure 1.1: Micro and nano material size. [14]

[18] The versatility of creating polymers allows researchers to optimize materials for solar energy absorption across various wavelengths. Despite these benefits, research remains in progress to solve issues with efficiency and long-term stability to make polymeric solar cells even more competitive with respect to existing solar technologies. [19]

1.2.1 Copper Zinc Tin Sulfur (CZTS) QDs

Cu_2ZnSnS_4 (CZTS) QDs are nanoscale semiconductor particles made from the elements copper (Cu), zinc (Zn), tin (Sn), and sulfur (S). CZTS QDs has received significant interest as a material with the potential to propel the advancement of cost-effective and high-performance PV technology. It has nontoxic and relatively cheap constituents. CZTS is an appealing alternative to conventional solar cell materials using cadmium or lead. CZTS-based manufacturing processes typically produce lower levels of environmental pollutants, aligning with a cleaner and greener approach to electricity production. [20]

CZTS has a promising PV property due to the direct band gap tunable in the range of 1.4–1.7 eV, which allows researcher to optimize its electronic properties for better absorption of sunlight and improved energy conversion efficiency in solar cells[1]. Additionally, CZTS has a very high absorption coefficient ($\sim 10^4$ cm^{-1}), making it an ideal candidate for the absorption layer in thin-film solar cells featuring multiple layer structures. [22] It is also possible to tune the properties of CZTS to enhance its performance in PV applications. Some of the properties that can be tuned are:

Figure 1.2: Chemical structure of CZTS (kesterite). [21]

1. Ionic substitution: Cation and anion substitution with Fe, Mn, and Se is implemented in CZTS to control the microstructure, band gap, and formation of the secondary phase in Cu_2ZnSnS_4 [23].

2. Size selection: The size of CZTS NCs directly impacts their optoelectronic properties. Size distribution can be controlled during the synthesis to optimize the spectrum for solar radiation, achieving enhanced light harvesting in solar cell applications. [24]

3. Post-treatment: Different post-treatments like thermal annealing and FLA can modify the structural and surface properties of CZTS NCs. [25] [26]

Despite the numerous benefits provided by CZTS material in PV applications, it is not exempt from certain challenges that demand solutions. Issues such as complex cation ordering that lead to deficits in open circuit voltage and reduced lifetimes of minority carriers need to be resolved. However, CZTS's potential for PVs in the future is still significant. These concerns are anticipated to be addressed by ongoing studies, establishing CZTS as a leading material for sustainable and efficient next-generation solar cell technology.

1.2.2 Poly(3,4-ethylenedioxythiophene) polystyrene sulfonate (PEDOT:PSS)

One of the polymers which is also very well known for PVs application is PEDOT:PSS. PEDOT:PSS is a heavily doped p-type semiconductor, with a bandgap of around 1.6 eV [34]. Highly conductive, but hydrophobic positively charged PEDOT core is surrounded by a negatively charged shell of hydrophilic PSS, forming a micelle structure. In such a way, PEDOT:PSS can be easily dissolved in water, making it very suitable for application [27] [28].

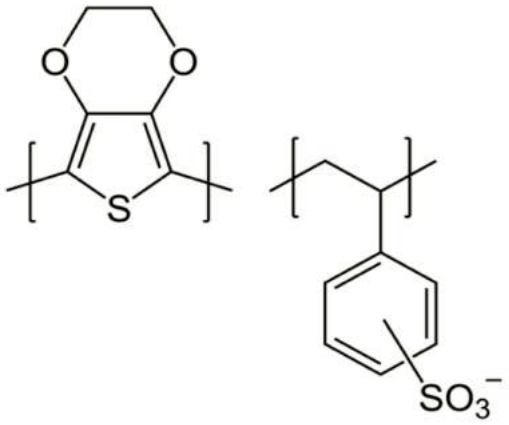

Figure 1.3: Chemical structure of PEDOT:PSS. [29]

PEDOT:PSS gained popularity in PV applications due to its high electric conductivity, flexibility, optical transparency, and solution processibility [30]. Within the realm of organic electronics, it functions as a component in a variety of devices—organic thin-film transistors, organic solar cells, and organic light-emitting diodes (OLEDs). The optical and electrical properties can be easily tuned through chemical or additive techniques and various post-treatments. This provides opportunities to alter its conductivity and transparency to meet specific requirements, with the ultimate objective of enhancing the device's overall efficacy. [31]

PEDOT:PSS, like many other materials, has several issues that need to be solved, such as stability, long-term performance, and larger-scale property optimization. Regardless of these difficulties, continuous research and efforts are focused on resolving these challenges. Furthermore, the combination of silicon and PEDOT:PSS in hybrid solar cells has gained popularity as it addresses some of the challenges associated with individual materials and provides opportunities for improved device efficiency and stability. The potential for PEDOT:PSS to contribute to the advancement of PV technologies remains high. [32]

1.3 Si/PEDOT:PSS Solar Cell

The global energy crisis has raised interest in solar cells. While crystalline silicon solar cells are prevalent, their significant cost makes it difficult to increase the solar power. Consequently, hybrid solar cells have gained importance, particularly those that combine silicon and organic materials—a process known as organic-Si hybrid solar cells, or HSCs. HSCs combine high efficiency and modern technology with a low-temperature production process, combining tunable optoelectronics of organic solar cells. Organic materials like Poly(3-hexylthiophene) (P3HT), graphene, PEDOT:PSS, and carbon nanotubes are used. Among the several organic materials, PEDOT:PSS has attracted a lot of research interest because of its remarkable qualities, which include high conductivity, transparency, good antireflection capabilities, efficient passivation, and widespread commercial availability. [33]

The Si/PEDOT:PSS hybrid solar cell has received interest because of its potential to achieve high efficiency, cost-effectiveness, and easy of fabrication. It is made of two different materials silicon and PEDOT:PSS. Silicon, a well-known semiconductor, acts as the light-absorbing material, with PEDOT:PSS serving as the hole transport layer [34]. This solar cell stands out for its aqueous solution processing. When comparing water-based solutions to traditional manufacturing processes, which often entail intricate and energy-intensive procedures, the former offers the advantage of being environmentally sustainable and capable of accommodating large-scale production. Recent research work has focused on the low complexity of the process, particularly the spin-coating of aqueous PEDOT:PSS solutions on n-type silicon surfaces followed by annealing. [35] The schematic structure of n-si/PEDOT:PSS solar cell is shown in Fig. 1.4.

The hybrid cell's power conversion efficiency (PCE) has been estimated to exceed 14 % for connections without antireflection coating, indicating its potential for high performance [37]. In the context of such hybrid solar cells, their performance depends on the effectiveness of the connection between silicon and PEDOT:PSS. A successful connection requires the minimization of defects at their contact, as a large

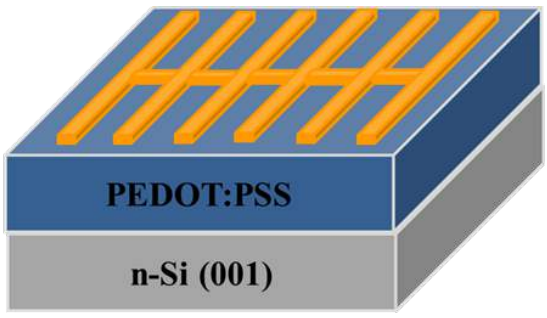

Figure 1.4: Schematic structure of planar hybrid n-Si/PEDOT:PSS solar cells. [36]

number of defects act as a barrier, preventing a smooth flow of electricity. Several factors influence the quality of this connection, including the composition that promotes PEDOT:PSS adhesion to silicon, the uniformity and thickness of the material layers, the presence of a natural layer on the silicon, the temperature during solar cell fabrication, and even the post-production storage conditions. [36]

1.3.1 Tuning Properties of PEDOT:PSS

Tuning PEDOT:PSS for solar cells is critical, as it serves as a hole-conducting layer in the manufacture of efficient solar devices. The conductivity of PEDOT:PSS has a significant influence on the accumulation of holes in the solar cell, which directly affects its overall performance. Researchers can improve charge carrier transportation inside the device by carefully modifying the composition and features of PEDOT:PSS, such as conductivity, wettability, and stability. This tuning is critical for improving power conversion efficiencies and ensuring long-term stability in solar cells. There are different ways to tune the PEDOT:PSS which are described below:

Solvent Treatment
Solvent treatment of PEDOT:PSS improves the efficiency of a solar cell via various mechanisms. PEDOT:PSS is made up of hydrophobic PEDOT and hydrophilic PSS, and while PSS helps PEDOT:PSS diffuse in water, it also reduces its conductivity. Researchers have the ability to alter the interaction between PEDOT and PSS by employing solvents like dimethyl sulfoxide (DMSO), ethylene glycol (EG), N,N dimethyl formamide (DMF), and tetrahydrofuran (THF). The inclusion of these solvents also improves conductivity and charge separation rates. This, in turn, results in higher values for critical parameters in solar cells, such as short-circuit current (JSC) and open-circuit voltage (VOC), leading to an overall rise in efficiency. [33]

Incorporation of N-Doped Carbon Quantum Dots
Another way to tune the properties of PEDOT:PSS is by adding nitrogen-doped carbon quantum dots (N-CQDs) to PEDOT:PSS. These N-CQDs enhanced the material's conductivity, altered its surface characteristics, and improved its structure. Computer simulations were utilized to demonstrate how N-CQDs help rearrange the molecules in PEDOT:PSS for improved performance. When combined with solar cells and light-emitting diodes, this modified PEDOT:PSS considerably increased their efficiency. [38]

There are different methods including the addition of QDs and nanotubes for the improvement in solar cell performance.

1. Incorporation of QDs: QDs improve solar cell performance by serving as the primary light-absorbing material in quantum dot-sensitized solar cells (QDSCs), collecting a wide range of light spectrum and creating excitons for opti-

mal light absorption. QDs help separate charges quickly, reduce energy loss, increase the lifetimes of charge carriers, and lower recombination losses, which increases the power conversion efficiency of QDSCs. [39]

2. Enhancing Solar Cell Efficiency with Carbon Nanotubes (CNTs): CNTs greatly enhance the efficiency of solar cells by acting as transparent and conductive front electrodes. This reduces optical shadowing and improves the absorption of light. There have been huge changes in the efficiency of solar cells that use CNTs along with silicon or other semiconductors, ranging from about 1% to as high as 14%. [40]

That's why in this work, we decided to mix CZTS QDs with PEDOT:PSS as CZTS, with its high absorption coefficient, is a potential PV material.

1.4 Deposition Techniques

Numerous deposition techniques exist and can be classified according to the physical state of the material being deposited, whether solid or liquid. Methods like physical vapor deposition (PVD), such as thermal evaporation and sputtering, are designed for depositing solid materials. In contrast, liquid-phase deposition techniques, like spin coating, spray coating, and dip coating are specifically tailored for depositing liquid materials. Each deposition method is chosen based on the desired material properties, substrate, and application requirements. [41] The most common deposition techniques are spin coating, spray coating, dip coating, drop casting, and sputtering. Each of these technique has advantages and disadvantages, which, together with the brief overview of the techniques by themselves, will be shown below.

1.4.1 Dip Coating

Dip coating is an easy and economical technique to deposite thin films. It involves dipping a substrate in a liquid solution. It is possible to regulate the thickness of the deposited layer by varying substrate withdrawal speed, solution concentration, and viscosity. After removing the substrate from the solution, a homogenous liquid is coated on its surface. As this film dries at room temperature, the volatile solvents evaporate, possibly causing chemical reactions that result in a thin coated film. Typically, the film requires heat treatment to undergo hardening or chemical transformation after being dried in a water atmosphere. [42] The dip-coating procedure is graphically illustrated in the Fig. 1.5 below.

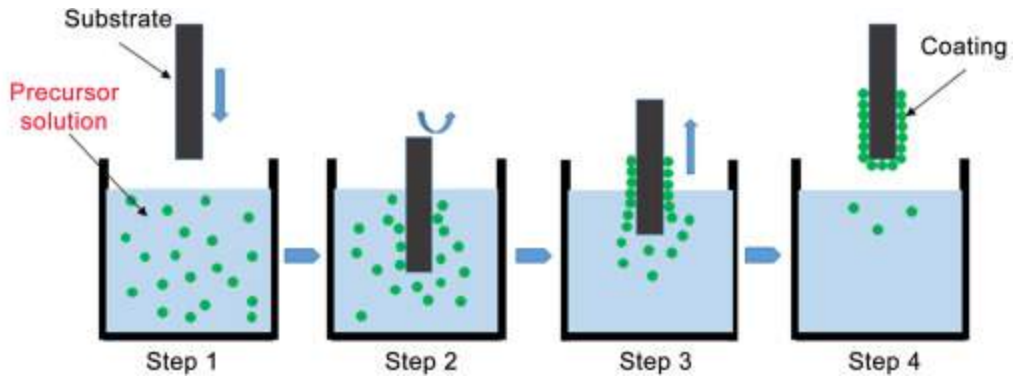

Figure 1.5: Graphical illustration of dip-coating method. [42]

Dip coating is commonly used for surface coating, in optics, and electronics with polymers, metals, ceramics, and composite materials. Dip coating has several benefits over other deposition methods, for example, cost-effective, straight forwardness, and the Capability to coat complex geometries. However, this technique has some limitations. For example, it is difficult to cover the substrate uniformly, especially for a non-wettable with the specific solvent surface. In addition, when ultra-thin (∼20 nm) or ultra-thick (∼1000 nm) layers need to be created, controlling the thickness becomes problematic [43]. Dip coating is suitable for producing large-scale films on various types of substrates, but the viscosity of the material solution and wettability of the surface limit its effectiveness. Despite these limitations, dip coating remains a popular and commonly used method for thin films deposition.

1.4.2 Drop Casting

Drop casting is one of the simplest film-forming techniques. Drop casting is the formation of a thin solid film (with a thickness from about 350 nm up to µm scale) by dropping a solution onto a substrate and then allowing the solvent to evaporate further. The schematic representation of the drop-casting procedure is displayed in Fig. 1.6. Using this technique, the thickness of the resulting film is determined by the concentration and the volume of the solution deposited.

Drop casting has the advantages of not necessitating complex processing stages or specialized equipment, and the deposition can be done at any atmosphere. There are no substrate or solution limitations, and it is relatively fast. This method, nevertheless, does have certain limitations. The main issue is the reproducibility of the film thickness, as sometimes it is quite challenging to deposit the same amount of material in exactly the same area. Also, it can be difficult to obtain uniform film thickness or particle distribution across large areas. Furthermore, the solvent evaporation process can cause undesired particle aggregation or film breaking. Drop casting is widely used to create thin films or patterns of nanoparticles or other

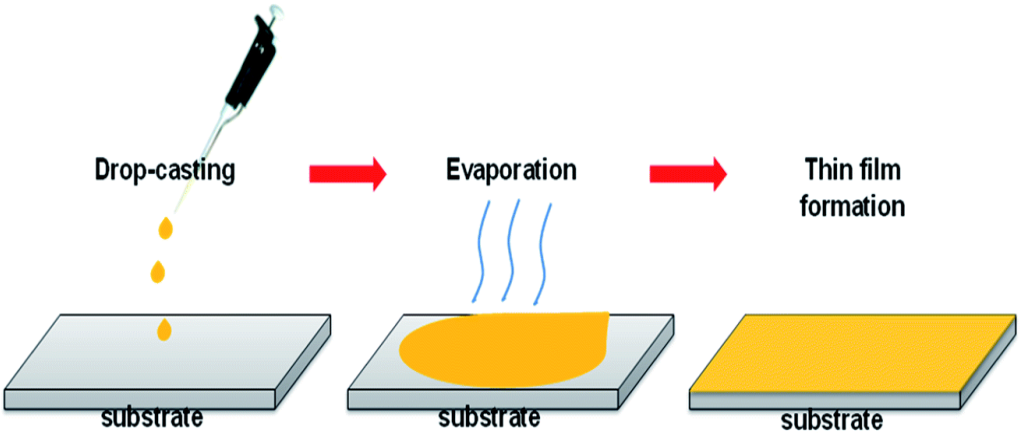

Figure 1.6: Schematic illustration of the drop-casting method. [44]

materials for different uses, such as chemical sensing, materials evaluation, and solar cells. It is a popular method among scientists for quick and easy sample preparation for further characterization. [45] [46]

1.4.3 Sputtering

Sputtering is often chosen over other physical vapor deposition (PVD) techniques for depositing thin films onto substrates because of its good quality film, highly controlled directionality, and lower absorption compared to other PVD methods [47]. Sputtering is a method used to create film coatings consisting of atoms that are sputtered from solid materials. The technique involves bombarding a target material, which is the material intended for deposition, with energetic ions. These ejected atoms are also known as sputtered atoms, which have high kinetic energy that helps them travel through the distance from target to substrate [48]. The schematic illustration of the sputter deposition set up is shown in Fig. 1.7.

There are several types of sputtering namely Direct Current (DC) sputtering, Radio Frequency (RF) sputtering, and magnetron sputtering. In DC sputtering, the power source is direct current whereas in RF sputtering, the power source is alternating current, and the power supply is a positive high-voltage radio frequency. Sputtering provides numerous benefits over other deposition techniques, including the capability to deposit a broad range of materials, attaining high-quality film, and consistency and excellent adhesion to the substrate. This method also enables precise film thickness, shape, and composition control [50].

The primary challenge in performing the sputtering process is maintaining a sufficiently strong plasma to produce a large supply of ions over the target's surface with a shape appropriate for the desired substrate surface [51]. Sputtering also has some restrictions including costly equipment and maintenance expenses, limitation

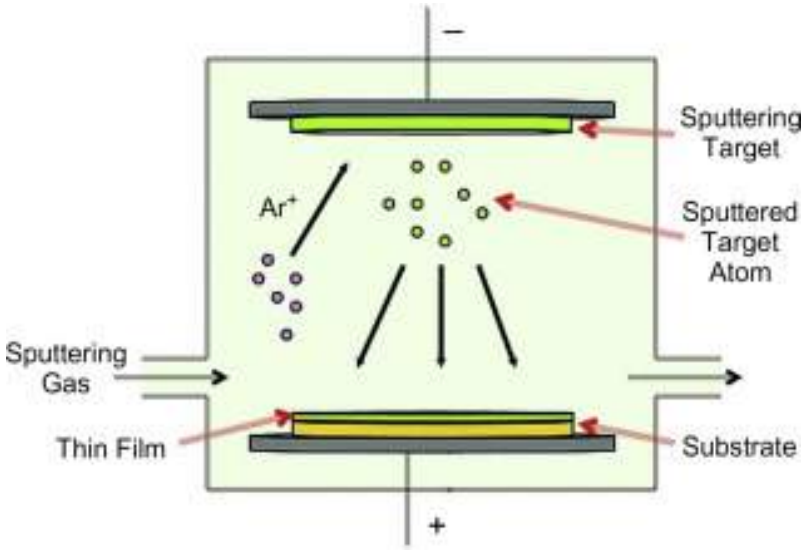

Figure 1.7: Schematic illustration of Sputter deposition setup. [49]

of target material, high vacuum requirement, and damaging of substrate due to ion bombardment. The majority of energy that strikes the target converts to heat, which needs to be released. Sputtering is a popular method for producing a variety of products, for example, integrated circuits, PV cells, magnetic sensors, and op tical coatings. It is also essential for producing flat-panel displays and hard disk drives. Despite its limitations, sputtering remains the main process for a wide range of industries and applications.

1.4.4 Spin Coating

Spin coating is a method of thin film deposition from liquid solutions by using centrifugal force. Originating in the field of microfabrication, this technique has been widely applied across other sectors because of its versatility and efficiency. The basic concept of spin coating includes the deposition of a liquid solution onto a substrate, followed by rapid spinning to disperse the solution uniformly throughout the surface. This process enables the creation of thin films with meticulous control over thickness, making it significant for the production of electronic components, optical devices, and solar materials.

The appeal of spin coating comes from its simplicity and effectiveness. Unlike many other deposition processes, which require complicated equipment or intricate procedures, spin coating provides a straightforward approach to achieve thin film coatings. Researchers and engineers can modify the properties of deposited films to meet individual requirements by varying factors like spinning speed, solution concentration, and spin duration. Furthermore, spin coating allows for the deposition

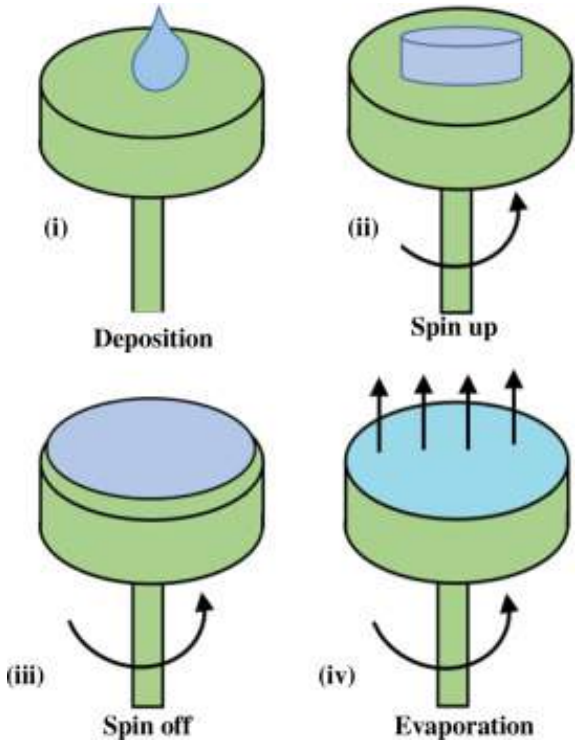

Figure 1.8: Stages of spin coating on substrate. [54]

of films with thicknesses ranging from less than 10 nm to several μm, making it appropriate for a variety of applications. [52]

Typically, the spin coating process can be categorized into four phases: deposition, spin-up, spin-off, and solvent evaporation as shown in the Fig. 1.8 [53] [54].

1. Deposition: During the deposition stage, the substrate is securely positioned on the spin coater, and a solution is applied to the substrate surface to completely coat it. This stage initiates the coating process, with characteristics such as solution viscosity and surface tension influencing solution spreading behavior. The substrate is then prepared for rotation, indicating the start of the subsequent phase.

2. Spin-Up: During spin-up, the spin coater device will be turned on, and the substrate will begin to spin until it reaches a particular speed. The centrifugal force produced by the substrate's acceleration and angular speed causes the flow of solution outward from the substrate surface. The solution thins out as it spreads, covering the substrate's surface in a homogeneous layer. Parameters like spin duration, acceleration, and rotational speed have significant effects on the spreading rate and uniformity of the solution.

3. Spin-Off: The third stage, also known as steady solution's thinning, begins

after the substrate is spinning at a constant rate and the excess solution is expelled from the substrate‘s edges. This removal of an excess solution leads to the formation of a uniform film thickness on the substrate. Factors such as viscous force, substrate surface properties influence the solution thinning and homogeneity.

4. Solvent Evaporation: The final stage, solvent evaporation, facilitates the drying of the thin film and determines the resulting thickness. As the spinning stops, solvent molecules continue to evaporate from the thin film until they are completely removed. This process results in the formation of a solid thin film adhered to the substrate's surface. Solvent properties, such as volatility and evaporation rate, as well as ambient conditions like temperature and humidity, all have a substantial impact on this stage.

So, the main parameters of the spin coating deposition that determine film thickness, roughness, and homogeneity are spinning speed, acceleration, spin time, number of steps and/or repeats, solution concentration, surface tension, and viscosity of the solution. Their variation allows to obtain the film with desired thickness and properties.

Spin coating has several advantages, including its ease of usage, speed, and cost-effectiveness. This technique is straightforward and readily available for depositing thin films, making it appropriate for researchers and engineers of various levels of experience. Furthermore, spin coating enables rapid manufacturing of thin films compared to alternative deposition processes, leading to greater productivity and efficiency. In addition, spin coating is an appealing option for projects with low budgets because it requires less resources and equipment. Furthermore, spin coating's versatility in depositing thin films for various applications, such as PVs and displays, further enhances its appeal, offering tailored solutions to meet diverse research and industrial needs. However, disadvantages of this method include difficulty in precisely controlling the film thickness, limited scalability, and the tendency for the film's edges to be thicker than the middle part. Additionally, the spin coating might be challenging to use on substrates that are non-wettable with the specific solvent. [55]

Applications of spin coating encompasses a wide range of industries, including the manufacture of PV devices, displays, and various electronic components. Spin coating improves visual quality by depositing uniform and defect-free coatings on display such as LCDs, OLEDs, and TFT arrays. Furthermore, spin coating is crucial in the production of electronic parts such as ICs, sensors, and microelectromechanical systems (MEMS), as it allows functional materials to be integrated onto substrates. All things considered, spin coating is essential to the advancement of technical innovation in the fields of information display, electronic device production, and renewable energy. [55]

As I used spin coating for my master's thesis work, which involves depositing PEDOT:PSS and CZTS on silicon substrates for solar cell fabrication, this technology's importance became even more evident. I achieved uniform and reproducible thin film deposition, laying the foundation for the manufacture of cost-effective and efficient solar cell devices. This accomplishment highlights the essential role that spin coating has played in the advancement of solar cell technology and emphasizes its ability to foster innovation in the realm of renewable energy.

1.4.5 Spray Coating

Another commonly used technique for thin film deposition from the liquid solution is spray coating, where, in general, the solution is force through a nozzle, resulting in the formation of a fine aerosol [56]. After the aerosol forms, droplets of the solution fall on the substrate, forming a thin film. There are different types of spray coating, namely thermal spray coating, high volume low pressure spray coating, plasma spraying coating, ultrasonic spray coating, and air spray coating. The spray coating method has several advantages:

1. Uniformity: The spray coating process can produce a uniform coating of the material on the substrate.

2. Efficiency and scalability: This approach is comparatively rapid and has the capacity to include large areas.

3. Control: By altering spray parameters such as solution concentration, spray rate, and substrate temperature, the technique provides for precise control over the thickness and composition of the layer being deposited.

4. High reproducibility: This method can produce consistent and repeatable outcomes in terms of the quality and characteristics of the coated thin films.

However, as with any other technique, spray coating also has some disadvantages:

1. It has several parameters that must be tuned to achieve the desired film.

2. It requires maintenance and cleaning during each experiment, especially to prevent clogging in the spray nozzle.

Spray coaters have been utilized for a range of applications, spanning from producing thin films for spectacles and screens in small areas to manufacturing large-scale thin film solar panels. Overall, spray coating is a cheap and flexible for depositing thin films with high control over thickness and homogeneity, making it a desirable choice for an extensive variety of applications [57].

During the optimization process of my solar cell design, I focused on using spray coating to deposit CZTS in order to improve the construction of layer-by-layer solar cells. This approach was critical in achieving consistent and reproducible coatings, which are essential for the reliable performance of the solar cells.

1.5 Post-Treatment Techniques

Post-Treatment process refers to the additional treatment applied to the materials after deposition. These approaches are intended to enhance specific characteristics, improve performance, or to achieve desired characteristics. In the context of thin film deposition, common post treatment techniques are thermal annealing, FLA and chemical treatments.

1.5.1 Thermal Annealing

Thermal annealing is a predominant technique to tune the properties of thin films. This approach includes treating the material to controlled heating at high temperatures, followed by a progressive cooling procedure. The fundamental objectives of thermal annealing are to optimize crystallinity, reduce internal stresses, and improve the overall quality of the thin film. During annealing, atoms or molecules in the material rearrange, resulting in defect reduction, higher grain development, and more homogeneity. The choice of annealing parameters, including temperature and time, is critical as it dictates the extent of modification and the final material character istics. Thermal annealing is widely used in many sectors, including semiconductor production, to improve electrical conductivity and optimize the performance of thin films in electronic devices. [58]

Throughout the experiment, I used thermal annealing extensively to improve the properties of PEDOT:PSS and CZTS films. The enhanced properties of these films significantly improved the efficiency and reliability of the solar cells, indicating the critical role of thermal annealing in advanced solar technology development.

1.5.2 Flash Lamp Annealing (FLA)

FLA is an alternative method of thermal annealing. Although it has been known for decades, the increased use of thin-film technology has caused it to become more well-known [26]. With FLA, a short-time annealing technique, high temperatures can be achieved at a substrate's surface or near-surface area in milliseconds, while deeper areas and the backside experience much lower temperatures. FLA systems typically

consist of a flash chamber and an energy storage system [59]. In this technique, the surface of the material absorbs a short yet powerful light pulse from a high-intensity flash lamp. The rapid absorption of energy generates a rapid temperature increase in the material, followed by a regulated and rapid cooling phase. This rapid thermal cycle contributes to certain material modifications such as crystallization, dopant activation, and stress release. FLA has several uses in a variety of sectors, most notably semiconductor production and thin film technology. [60]

During the experiment, I used the FLA technology to achieve rapid and precise heating and cooling cycles for PEDOT:PSS and CZTS thin films. The successful application of FLA revealed its significance, which were fundamental to the advancements in my research.

1.6 Characterization Technique

1.6.1 Raman Spectroscopy

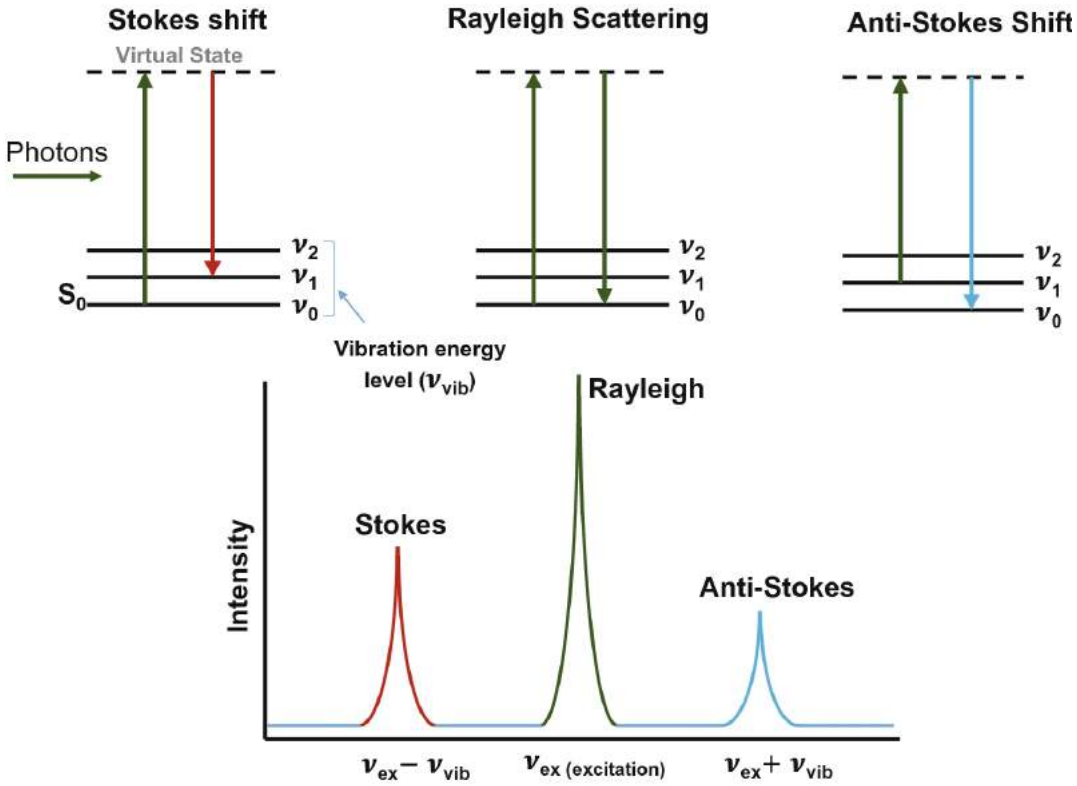

Figure 1.9: Rayleigh and Raman Scattering. [61]

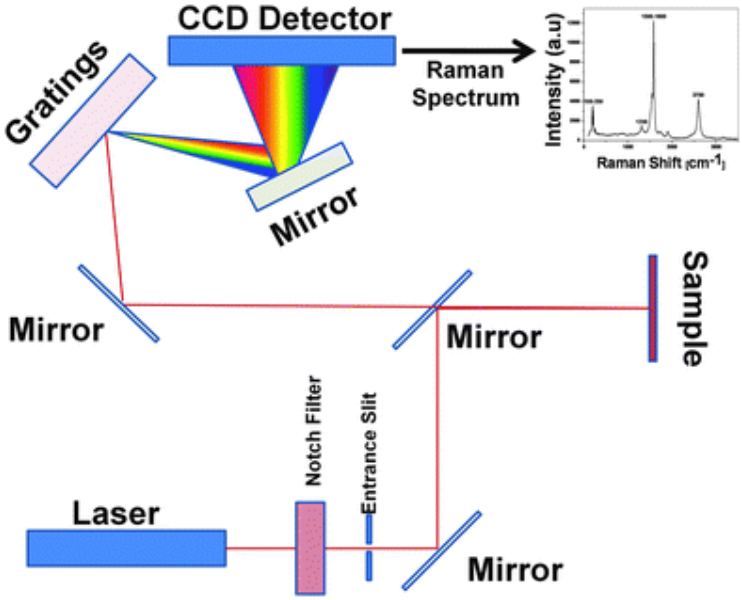

Figure 1.10: A schematic diagram of Raman spectroscopy setup. [63]

Raman spectroscopy is a characterization technique used to identify molecular and crystalline structures by observing the frequency shifts in light that is inelastically scattered after interacting with a sample. This technique determines if the scattered light exhibits a lower frequency, referred to as Stokes Raman scattering, or a higher frequency, called anti-Stokes Raman scattering as shown in Fig. 1.9. [62] Most Raman spectrometers utilize Stokes Raman scattering, where the wavelength of incident light shifts according to the unique vibrational energy of each molecule. This shift allows for the identification of a substance's chemical composition or structure through its distinct scattering patterns. [61]

A Raman spectrometer operates by focusing laser light onto a specimen and collecting the light that is scattered back. Filters selectively remove the intense Rayleigh scatter, allowing only the Raman-scattered light to pass through. The monochromator disperses the light and the CCD detects it, analyzing the wavelengths to identify the molecular composition of the sample. The schematic diagram of Raman spectroscopy set up is shown in Fig. 1.10.

2 Instrument and Techniques

2.1 Spin Coating

In the experiment conducted, spin coating was utilized to deposit PEDOT:PSS and a mixture of PEDOT:PSS with CZTS onto a substrate. Initially, the substrate was cleaned as mentioned in Chapter 3.1.3 and firmly positioned on the chuck of the spin coating device. The substrate was then stabilized in position by creating a vacuum beneath it through the activation of a vacuum pump. Subsequently, a two-step procedure was employed to establish the device parameters.

In the first step, the speed and acceleration were set to 2000 revolutions per minute (rpm) and 500 rpm/s, respectively, for a time period of 20 seconds. Moving on to the second step, the duration of rotation was established as 10 seconds, with a 3000 rpm rotation speed and an acceleration of 1000 rpm/s. Approximately 50 µl of solution was dropped on the substrate. The huge centrifugal force induced during the spin coating process facilitated an even distribution of the solution across the substrate, ensuring a uniform coating.

In this project, spin coating MODEL WS-650MZ-23NPP/LITE was used. The schematic structure and the photo of the one used is displayed in Fig. 2.1 and Fig. 2.2 respectively. In our case, spin coating system located inside the hood (Fig. 2.2) provided exact control of the speed, number of steps, and time required to achieve

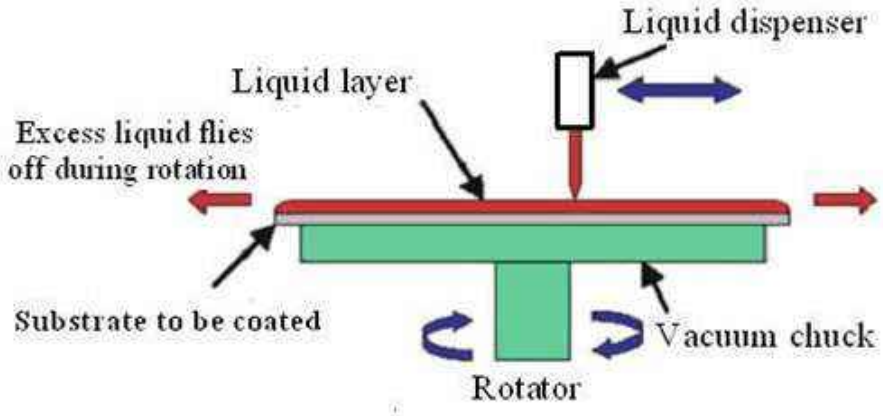

Figure 2.1: Schematic structure spin coating. [64]

Figure 2.2: Spin coating used for this project.

a uniform thin film.

To obtain high quality homogeneous thin film, it is important to remove bubbles while dropping the solution on the substrate to ensure uniform solution coverage for the consistent thickness.

2.2 Ultrasonic Spray Coating

In my master thesis experiment, a spray coating device was employed to deposit CZTS on a silicon substrate. The cleaned substrate was placed on the sample holder. In our case, the spray-coating was system located in the glove-box (Fig. 2.4) with a nitrogen atmosphere configured with precise control over several parameters to achieve the desired film properties. The nozzle height was set at 3.8 cm, and the nozzle speed was set at 2 mm/s. The flow rate was kept 10 mL/hr, and the substrate temperature was maintained at 90 °C. Additionally, the number of spraying cycles was set between 5, 7, and 10 to obtain the film with uniformity and high reproducibility.

In the experiment, Ultrasonic spray coating Sono-Tek 06-5108 was used. The general schematic view of spray coating systems and photo of one used in this work are shown in Fig. 2.3 and Fig. 2.4 respectively.

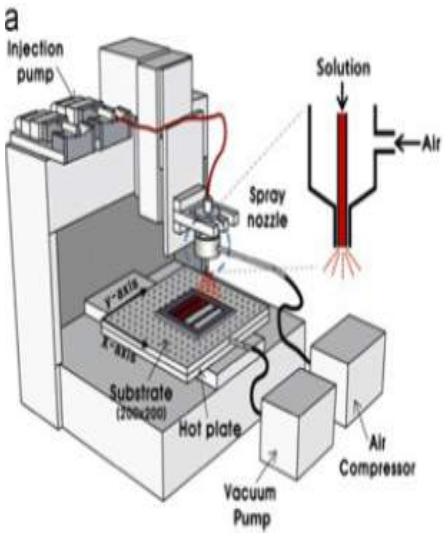

Figure 2.3: Schematic diagram of spray coater. [65]

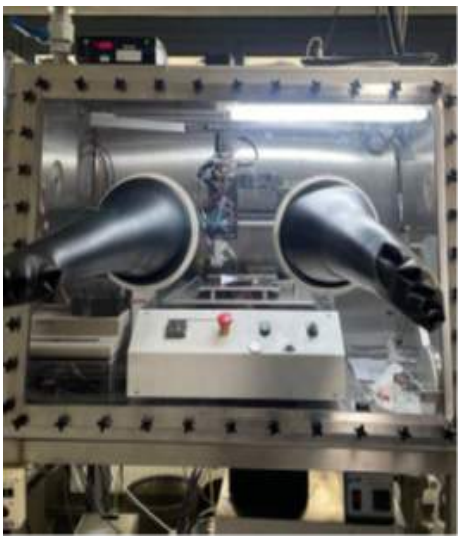

Figure 2.4: The photo of spray coater used for this project.

2.3 B 30 – Thermal Evaporator

In my experiment, gold was deposited using a B 30 thermal evaporator, with gold wire serving as the source material. The experiment started by activating the diffusion pump's heating by pressing F1, followed by a waiting time of one-hour. The chamber was opened, the sample was inserted, and the glass plate was cleaned. After sealing the chamber and setting it to low vacuum, evaporation commenced once the left gauge displayed less than 10 µA. The current was slowly increased to melt and evaporate the gold. The process concluded with the deactivation of the diffusion machine and a cool down period before safely removing the sample.

In this study, thermal evaporator B 30.2 Erz.-Nr. 513902 from VEB JOCHVAKUUM DRESDEN was used. The general schematic view of thermal evaporator and the photo of one used in this work is shown in Fig. 2.5 and Fig. 2.6 respectively.

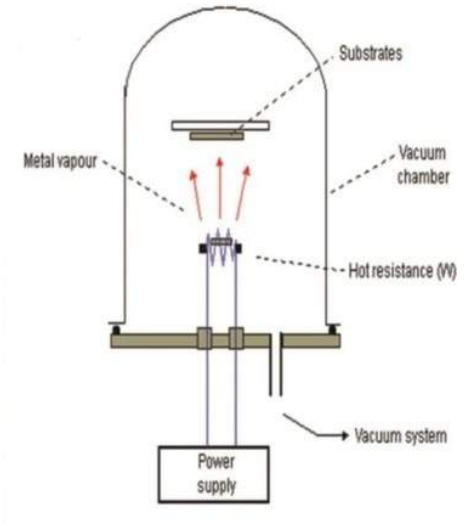

Figure 2.5: Schematic view of a thermal evaporator. [66]

Figure 2.6: B-30 thermal evaporator unit used for this study.

2.4 Heating Plate

During the experiments, a heating plate was used for thermal annealing. This procedure was conducted inside a glove box, which is designed to maintain a specifi atmospheric condition. The samples were placed directly on the heating plate, and the heating switch was activated. The temperature settings were precisely calibrated to meet the exact requirements of the annealing process, ensuring optimal conditions for the desired chemical and physical changes. In our case, annealing procedure was carried out across three different temperatures: 75 °C, 100 °C, and 150 °C for a duration of 25 minutes, which was determined to be sufficient for achieving the desired outcomes. After this amount of time, the heater was turned off, which ended the annealing process. After that, the samples were carefully taken off the hot plate so they could be analyzed further or used in other experiments.

The heating plate used in this project is a product of Heidolph Instruments, model MR 3001 K. The photo of the device used in this experiment is shown in the Fig. 2.7. The employment of this heating plate model was essential for successfully completing the thermal annealing phase, contributing significantly to the overall outcome of the research.

Figure 2.7: The image of heating plate used in the experiments.

2.5 Flash Lamp Annealing Set Up

In this project, FLA setup was an important technology used in our experimental approaches. The FLA system, which was installed inside a glove box to ensure an inert atmosphere, was critical in processing the samples. The instrument contains a FLA chamber that can be removed for sample placement. After positioning the sample, the chamber was closed again, resulting in an enclosed environment prepared for annealing. After turning on the control system, the energy density parameters were carefully set to meet the needs of the annealing process, ensuring optimal conditions for the material transformation. Once the system was ready, as shown by the control interface, the annealing process was started by pressing a button. An audible boom marked the completion of the process. This was caused by the intense flash from the Xenon light, which shows the fast energy discharge that is characteristic of the FLA technique. This process's immediacy not only saves time but also reduces thermal exposure, conserving the sample's substrate. Once the flash was completed, the chamber was opened and the sample was taken out for further analysis.

In this work, a FLA setup, sourced from Dresden Thin Film Technology GmbH (SOLAYER GmbH, Kesselsdorf, Germany), was used. The photo of the FLA chamber and control system is shown in Fig. 2.8 and Fig. 2.9 respectively.

Figure 2.8: FLA Chamber.

Figure 2.9: FLA control system.

2.6 Solar Simulator for Electrical Characterization

Figure 2.10: Solar simulator used for this work.

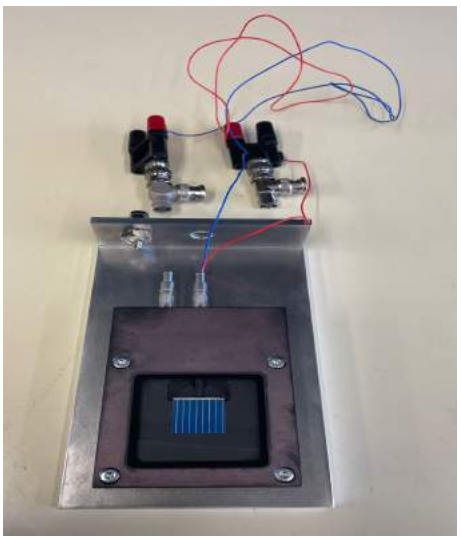

Figure 2.11: Standard silicon (Si) reference solar cell.

Solar simulators are essential tools in scientific research, especially for studying PV cells. It replicates the intensity and spectral composition of natural sunlight for controlled testing of materials and devices sensitive to light [67]. The solar simulator extracts the current-voltage (IV) curve, which demonstrates the electrical behavior of a solar cell. The IV curve typically includes information on the maximum power point (MPP), open-circuit voltage (Voc), and short-circuit current (Jsc) for optimizing solar cell design and performance.

The Sun 2000 solar simulator from Abet Technologies was used for the characterisation technique. Solar simulator that was used for this study is shown in Fig. 2.10. This specialized equipment provides controlled illumination for testing solar cells. To assure test reliability and precision, the solar simulator's illumination power was calibrated with a standard silicon (Si) reference solar cell shown in the Fig. 2.11.

2.7 XploRA Raman Microscopy

Xplora Raman microscopy was used in the experiment to investigate the molecular composition of PEDOT:PSS film. Measurement was initiated by powering the microscope to ensure that all system components were operational. The laser, which serves as the essential light source for Raman scattering, was then activated. The connected software on the computer was started, which is required for controlling the microscope and managing the data.

Once the system was operational, the software interface was used to modify the camera settings to properly position and focus the sample under the microscope. The appropriate acquisition parameters, such as the spectrum window, were set. The overall instrumental setup was checked to ensure that everything was aligned and functioning correctly. Before beginning actual measurements, an auto calibration was conducted to confirm the accuracy of the Raman shift data. Following this calibration, the device was ready to collect comprehensive Raman spectra for molecular analysis.

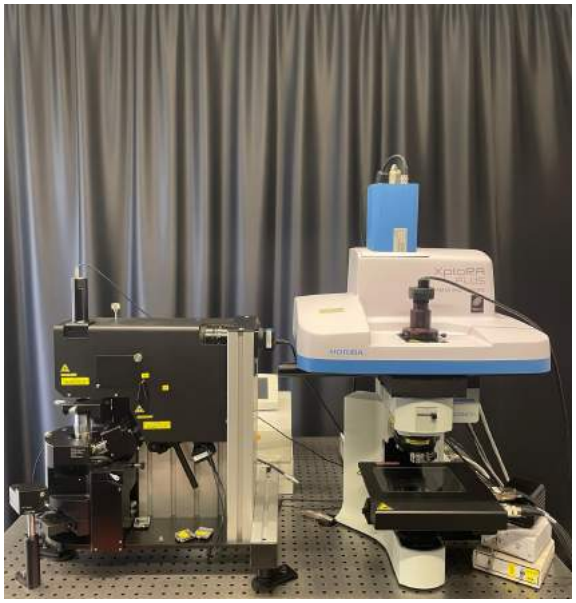

Figure 2.12: XploRA Raman Microscopy used for this project.

In this study, Raman spectroscopic analyses were conducted using the XploRA PLUS Raman microscope from HORIBA, as depicted in Fig. 2.12. The apparatus was situated within a controlled cleanroom environment to ensure contaminant-free conditions and maintain the integrity of the sample measurements.

2.8 Choice of the Substrate

In this project, a silicon substrate of n-type, double-side polished (dSP) with a thickness of 400 micrometers and a (100) crystal orientation was used. It has an electrical resistivity of 1-4 Ω-cm, making it appropriate for various semiconductor applications. The main reason for using silicon substrate was to create a p-n junction, with n-type silicon, doped with arsenic, facilitating electron transport and p-type organic semiconductor PEDOT:PSS functioning as a hole transport material, hence optimizing charge separation and increasing solar cell efficiency.

Furthermore, its abundance and low cost make solar cell fabrication economically viable. The bandgap of silicon is 1.1 eV, which can be tuned further corresponds to the energy of photons in the visible and near-infrared regions of the solar spectrum. [68]

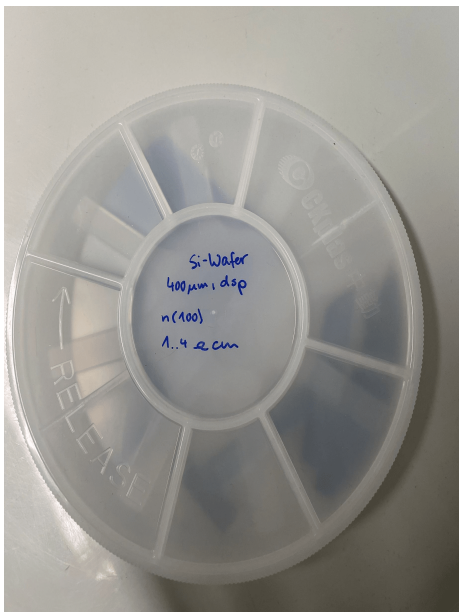

Figure 2.13: Silicon wafer box with details used for this work.

Figure 2.14: Silicon substrate

Another significant benefit is that silicon is suitable with a range of deposition methods, such as chemical vapor deposition (CVD) and physical vapor deposition (PVD), facilitating the integration of multiple layers and materials required for

solar cell fabrication. The silicon wafer box and the silicon substrate used in the experiment are depicted in Fig. 2.13 and Fig. 2.14 respectively.

2.9 Software for Data Analysis

In this work, for processing the data from the solar simulator, Origin Pro 2024 software was used. Origin software offers a comprehensive and user-friendly platform for analyzing and visualizing data, making it a valuable tool for evaluating the performance of solar cells. It was crucial for creating graphical representations, specifically the current-voltage (I-V) curve. The software was used to determine the solar cell's efficiency, which is a critical parameter that indicates the effectiveness of converting incident light into electrical energy.

3 Synthesis and Design of Solar Cells

3.1 Sample Preparation

The preparation of a solar cell involves the following steps to create a device capable of converting sunlight into electricity:

1. Synthesis of CZTS
2. Preparation of PEDOT:PSS
3. Cleaning the substrate
4. Deposition of PEDOT:PSS and CZTS composite by spin coating
5. Post-treatment
6. Gold Deposition and In/Ga eutectic as back contact

3.1.1 Synthesis of CZTS

There are various methods to synthesis CZTS NCs. Typically, CZTS are produced by well-known method like hot injection in organic solvent or thermolysis of a single precursor. These methods offer meticulous control over the dimensions (size), form (shape), and composition of nanocrystals. Hydrothermal/solvothermal methods and microwave-assisted techniques are commonly used for photocatalysis applications [69] [70] [71] [72]. However, these methods often require post-synthesis treatment, including phase transfer into the water. There is a need for easier approaches, such as producing CZTS nanocrystals directly in water. For this reason, we mainly focused on "green" aqueous synthesis which uses mercaptoacetate (MA) anion to stabilize the colloidal CZTS NCs. [2]

"Green" Aqueous Synthesis
This method is a simple and low cost method that allows us to have greater control and insight into the properties of CZTS particles, making them potentially useful for various applications.

Materials: Mercaptoacetic acid (MAA), $Cu(NO_3)_2$, $SnCl_2$, $Zn(NO_3)_2$, Na_2S, Isopropanol, Deionized (DI) water

Procedure: Initially in the synthesis process, a beaker containing a tiny magnet was used. DI water (6 mL) was poured into the beaker and placed on a rotating plate at a speed of 900 rpm. To the spinning solution, 0.3 mL of $Cu(NO_3)_2$, 0.15 mL of $Zn(NO_3)_2$, and 0.3 mL of $SnCl_2$ were added under control. Then, 3 mL of MAA was quickly added to the mixture to complex the metal ions. This complexation was important because it prevents the premature precipitation of the metals and ensures that the NCs grew in a controlled manner. The observed solution after the addition of MAA is shown in Fig. 3.1.

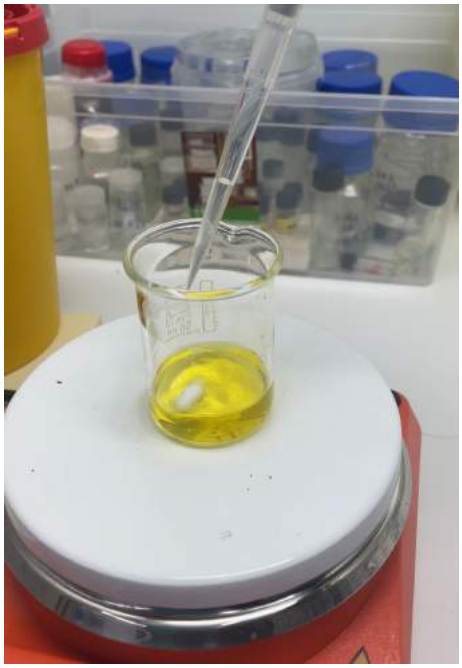

Figure 3.1: Solution after the addition of MAA.

Then 0.3 mL of Na_2S was added all at once. The sulfide ions reacted with the metal complexes to initiate the formation of CZTS nanocrystals. The sulfide ions provided the necessary sulfur component of the CZTS crystal structure. To avoid the solution precipitating too soon, the reaction was carefully monitored. The observed solution after the addition of Na_2S is shown in Fig. 3.2.

Prior to moving to the next stage, the magnet was removed and the solution was then transferred to two test tubes. Each tube receives 5 mL of isopropanol, and the solution underwent centrifugation for a duration of 5 minutes at 5000 rpm. Following this procedure, CZTS nanoparticles precipitated. Afterwards, the liquid and residue were separated. These steps are shown in the Fig. 3.3, 3.4, and Fig. 3.5.

Figure 3.2: Solution after the addition of Na_2S.

Figure 3.3: Addition of isopropanol.

Figure 3.4: Centrifugal device.

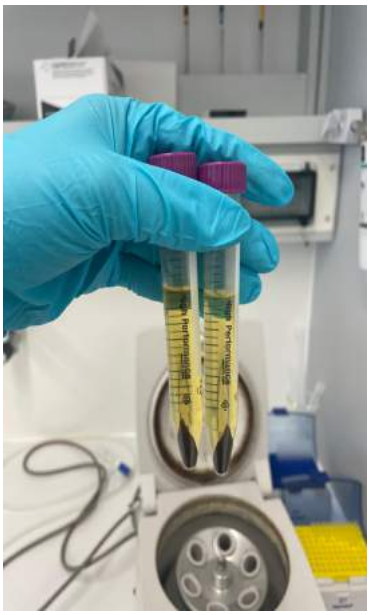

Figure 3.5: Solution after centrifugation.

Finally, 0.4 mL of DI water was added to the residue and the entire mixture was well shaken. A 1 mL combination of residue and distilled water containing the produced CZTS nanoparticles was the resultant solution as shown in the Fig.

3.6. This comprehensive synthesis procedure assured the controlled synthesis and concentration of CZTS nanoparticles, which makes it appropriate for a range of PV and nanotechnology applications.

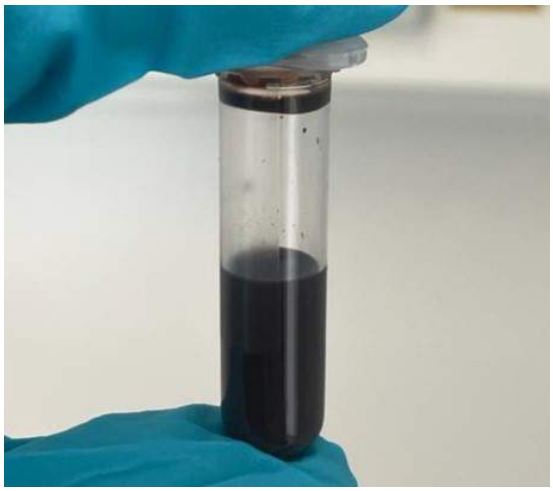

Figure 3.6: CZTS NCs solution prepared by this method.

3.1.2 Preparation of PEDOT:PSS

In the preparation of PEDOT:PSS, a systematic procedure was employed. Initially, the concentrated PEDOT:PSS commercially available solution was ultrasonicated for 10 minutes. Following this, sodium dodecyl sulfate (SDS) and dimethyl sulfoxide (DMSO) were added to the solution. SDS acts as a surfactant in the PEDOT:PSS solution, effectively reducing the surface tension and enhancing the wetting characteristics. This surfactant action helps to enhance the homogeneity of the resultant thin film. On the other hand, DMSO acts as a solvent, aiding in the uniform dispersion of PEDOT:PSS during film deposition, resulting in smoother films. Its presence enhances the electrical conductivity of PEDOT:PSS films, allowing for improved charge transfer within the polymer matrix.

10 % solution of SDS was made. For this, 1 g of SDS was dissolved in 10 mL of DI water, and the solution was shaken well and then sonicated. The prepared SDS solution is shown in the Fig. 3.7.

Following this step, 5 vol% DMSO and 2.5 vol% SDS were added to the PEDOT:PSS solution. The mixture was ultrasonicated for 5 minutes. In order to further purify the solution, a poly(vinylidene fluoride) membrane with a porosity of 0.45 μm was used in the filtration process.This filtering step was done to remove agglomerations and assure a pure solution, making it ideal for applications requiring high conductivity and surface uniformity. The mixture of PEDOT:PSS, SDS, and DMSO solution is shown in Fig.3.8.

Figure 3.7: SDS solution.

Figure 3.8: Mixture of PEDOT:PSS, SDS, and DMSO.

3.1.3 Cleaning the Substrate

The silicon substrate was prepared and cleaned in a precise sequence of steps. The Si samples (1×1 cm^2) were cut from the silicon wafer. Subsequently, the silicon substrate was immersed in 40% hydrofluoric (HF) acid for 1 minute, effectively removing the native oxide layer. Following the acid treatment, the substrate was thoroughly rinsed in DI water and dipped twice to ensure that all remaining acid was removed. The substrate was then carefully dried on both sides with a stream of nitrogen gas.

3.1.4 Deposition of PEDOT:PSS and CZTS Composite by Spin Coating

Following a thorough cleaning of the substrate, we mixed PEDOT:PSS and CZTS, varying the volume of CZTS in each combination. The solution had to be mixed immediately before being applied to the substrate since it tended to form clumps over time, a process known as agglomeration. This agglomeration phenomenon became visible roughly 30 minutes after mixing, and the level of agglomeration depends on the amount of CZTS added to the PEDOT:PSS. After carefully preparing the solution, we used spin coating to deposit it on the silicon substrate. The film deposited on the substrtae is depicted in the Fig. 3.9.

Figure 3.9: Deposition of PEDOT:PSS and CZTS.

3.1.5 Post-Treatment

Following the deposition process, the samples were separated into two subsets for annealing treatments to facilitate a comparative analysis. The first subset underwent thermal annealing, where the temperature was systematically varied from 75 °C to 150 °C. This treatment enhanced the crystallinity of PEDOT:PSS by aligning PEDOT chains and promoted the growth of well-defined crystalline domains in CZTS, thus improving the kesterite structure [73]. The second subset was subjected to FLA, with energy densities ranging from 8 J/cm² to 18 J/cm². FLA is utilized to heat the material surface with intense light pulses, a crucial step in semiconductor processing for activating dopants, reducing defects, and inducing controlled modifications with minimal thermal impact on the materials. [74]

3.1.6 Gold Deposition and In/Ga Eutectic as Back Contact

To evaluate the PV properties, a gold grid pattern was thermally evaporated onto the surface of the composite PEDOT:PSS and CZTS layers.This process was carried out using a shadow mask, as depicted in Fig. 3.10. The gold (Au) top contact acts as a pathway for electrons generated within the PV device, allowing for effective current collection and charge transport. Furthermore, an indium (In)/gallium (Ga) eutectic was scratched on the silicon substrate as a back contact as shown in Fig. 3.11. It creates a strong electrical connection at the back of the substrate, improving the device's overall conductivity and performance.

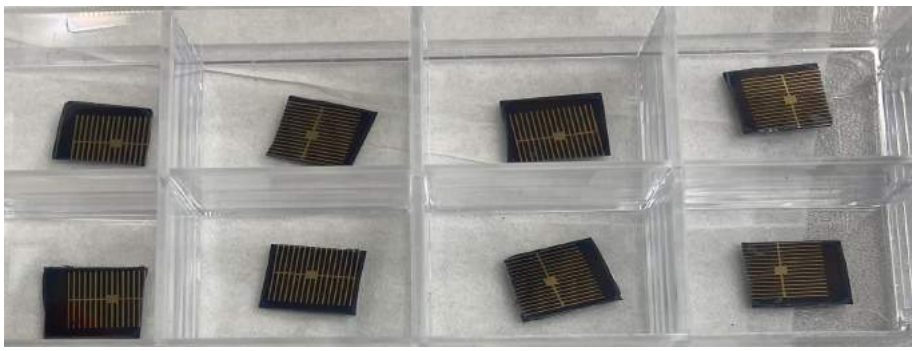

Figure 3.10: Samples after gold deposition.

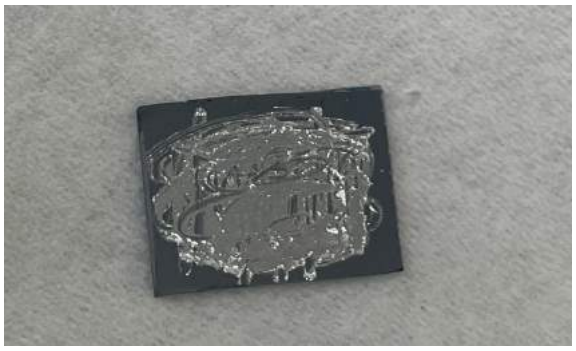

Figure 3.11: Scratched on the backside of sample using In/Ga.

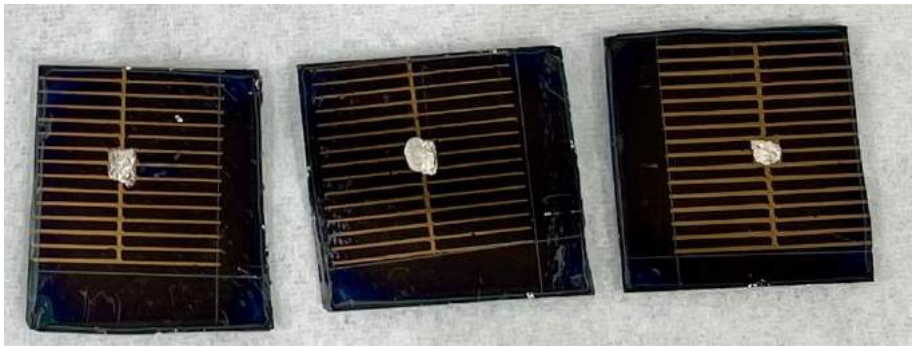

Figure 3.12: Image of the solar cell samples

Additionally, silver (Ag) paste spots were carefully added to the middle of the sample as shown in Fig. 3.12, functioning as localized contacts for precise electrical connections. By combining these materials and techniques in a strategic way, we were able to carefully produce our sample and do a thorough evaluation and study of its PV performance and properties.

3.2 Working Principle of Solar Cell

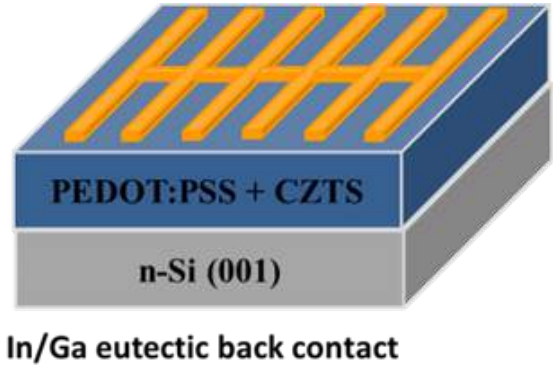

Figure 3.13: Schematic of Solar cell. [36]

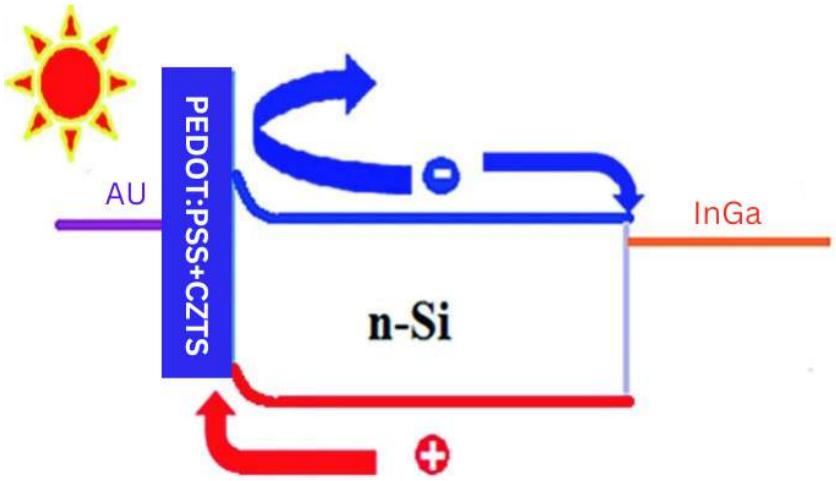

Figure 3.14: Schematic band diagram of n-si/PEDOT:PSS-CZTS solar cell. [75]

The multilayered structure of the solar cell shown in the Fig. 3.13 is created to efficiently convert solar energy into electrical energy. Each of the layers has its own specific objective to enhance the efficiency of the photovoltaic system. The schematic band diagram of n-si/PEDOT:PSS-CZTS solar cell is shown in Fig. 3.14. The cell's base is an n-type silicon (n-Si) substrate, which is doped with elements that add electrons to the silicon lattice, resulting in an electron-rich environment. This n-Si layer is the primary photon absorber from sunlight. When photons with sufficient energy strike silicon substrate, they can excite electrons from their atomic orbitals, creating electron-hole pairs. The electrons are the negative charge carriers, while the holes act as positive charge carriers in the material.

The PEDOT:PSS-CZTS layer is located just above the silicon substrate. PEDOT:PSS is an electrically conductive polymer with numerous applications. Its pri-

mary function is that of a hole transport layer, allowing the holes that are created in the silicon to migrate up towards the cell and be collected there. Additionally, at the interface with the n-Si, it creates a Schottky barrier. A Schottky barrier is a potential energy barrier for electrons formed at the junction between a metal and a semiconductor, arising from the differences in their work functions [76]. This barrier helps in the separation of charge carriers by allowing holes to pass through to the PEDOT:PSS layer while resisting electrons, thereby preventing recombination where the generated electrons and holes annihilate each other.

The inclusion of CZTS, a semiconductor with a bandgap tuned to absorb a broad spectrum of sunlight, improves the cell's absorption capacity. The integration of CZTS allows the solar cell to use more of the sunlight spectrum, potentially leading to higher conversion efficiencies.

The top contact is made of gold (Au). It was chosen for its good conductivity. This layer provides the pathway for the electrons generated in the n-Si to travel to an external circuit. The contact is patterned, often in a finger-like configuration, maximize electron collection while minimizing surface area coverage, allowing as much light as possible to reach the active layers beneath. Finally, an Indium/Gallium (In/Ga) eutectic, a liquid alloy of indium and gallium, was utilized. It remains in a liquid state at normal room temperature. This material was frequently employed to create a reliable electrical connection between the semiconductor and a metal electrode. In this solar cell, it was used for the collection and transportation of positively charged holes from the PEDOT:PSS layer to an external circuit. This completed the electrical circuit, allowing current to flow through the electron-hole pairs formed by photon absorption.

After the fabrication of solar cell, it was electrically characterized by solar simulator. We prepared two identical samples to measure their efficiency and fill factor (FF), which allowed us to calculate the error bars representing the variability in these measurements.

The efficiency of solar cells is the percentage of incoming sunlight that can be converted into useful electrical energy. It is denoted by η. The formula to calculate the efficiency is:

$$\eta = \frac{U_p J_p}{P_0} \times 100\ \% \tag{3.1}$$

where,

η : Efficiency
U_p : is the voltage at maximum power point.
J_p : is the current density at the maximum power point.
P_0 : is the input power, typically the power of the incident sunlight, measured in watts per square meter (W/m^2).[77]

FF is a dimensionless number that measures the 'squareness' of the solar cell's IV curve. It effectively rates the quality of the solar cell. The formula to calculate the FF is:

$$FF = \frac{U_P J_p}{U_{os} J_{sc}} \tag{3.2}$$

where,

FF : Fill Factor
U_p : is the voltage at maximum power point.
J_p : is the current density at the maximum power point.
U_{os} : is the voltage at which there is no current flowing through the device.
J_{sc} : is the current at which there is no potential difference across the solar cell.[78]

4 Result and Discussion

4.1 Optimizing Post-Treatment Parameters for Silicon/PEDOT:PSS Solar Cells

During the initial stage of our experimental investigation, we focused only on the deposition of PEDOT:PSS onto silicon substrates without introducing CZTS. This decision was driven by the need to initially establish a set of optimum settings for the pure PEDOT:PSS layer, which acts as an essential part of our solar cell structure.

4.1.1 Electrical Characterization of Si/PEDOT:PSS Solar Cell Varying Temperature of Thermal Annealing

In this particular experiment, pure PEDOT:PSS was deposited by using spin coating technique followed by thermal annealing at varying temperatures of 75 °C, 100 °C, and 150° C to investigate their impact on PEDOT:PSS film properties and the overall device performance.

A comparative analysis of the PEDOT:PSS solar cell efficiencies post thermal annealing at different temperatures demonstrated a noticeable trend. At 75 °C (Fig. 4.1a), the cell produced the highest efficiency of 4.82 %. When the annealing temperature was increased to 100 °C (Fig. 4.1b), a small drop was noted, reaching 4.64 %. Further raising the annealing temperature to 150 °C (Fig. 4.1c) resulted in an efficiency of 4.24 %, confirming the trend of decreasing returns at higher temperatures.

This finding indicates that the thermal annealing treatment significantly impacts the structure and electrical properties of PEDOT:PSS film. The decrease in efficiency at higher annealing temperatures was caused by thermal degradation of the PEDOT:PSS layer.

According to the literature [79], annealing the PEDOT:PSS layer at high temperatures has mixed effects on device performance. While it leads to a slight increase in JSC, it also causes a decrease in fill factor. These modifications could be related to variations in the PEDOT:PSS layers' conductivity and surface roughness caused

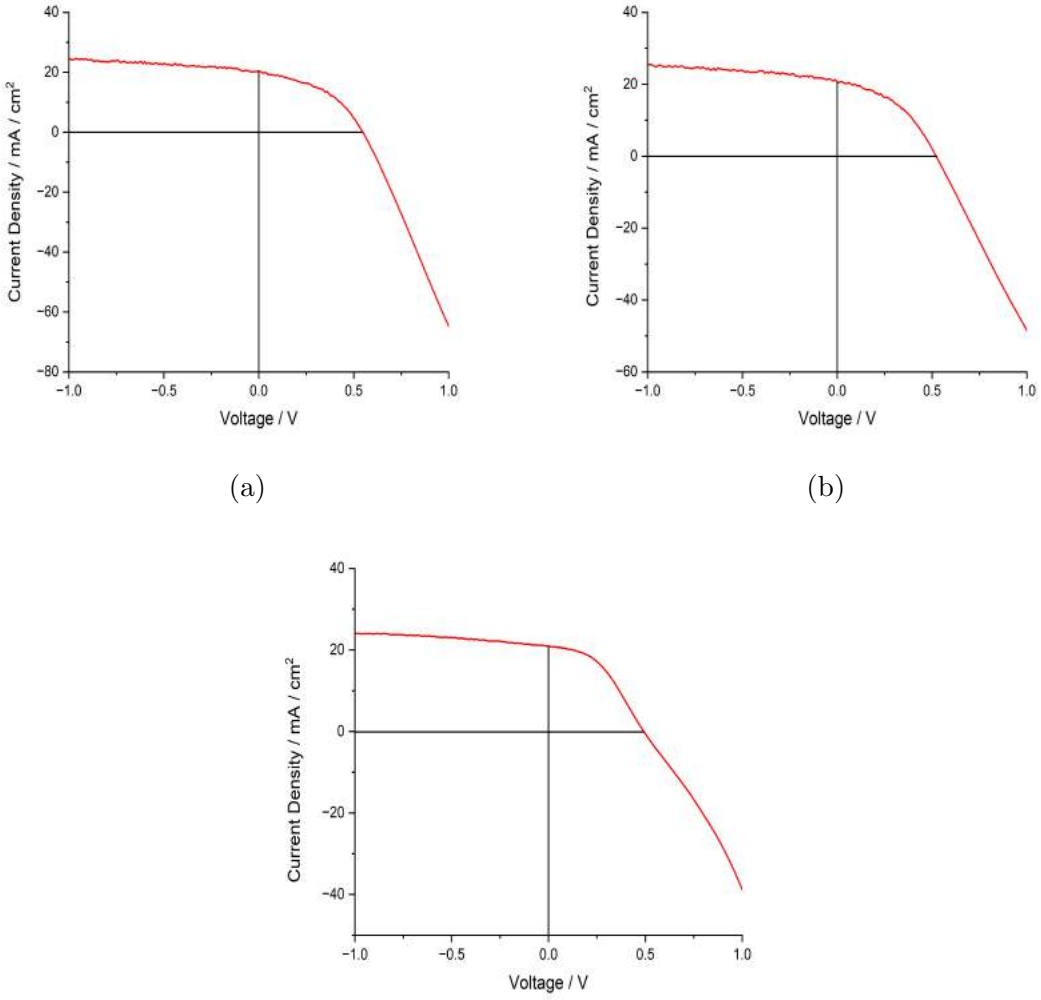

Figure 4.1: Illumination J-V characteristics for n-Si/PEDOT:PSS solar cell treated by Thermal Annealing at (a) 75 °C (b) 100 °C and (c) 150 °C.

by heat treatment.

The efficiency and fill factor calculation at 75 °C shown in **Fig. 4.1a** is:

$\eta = \frac{U_p J_p}{P_0} \times 100\ \% = (4.82\ \pm\ 0.06)\ \%$

$FF = \frac{U_p J_p}{U_{os} J_{sc}} = 0.44\ \pm\ 0.01$

The efficiency and fill factor calculation at 100 °C shown in **Fig. 4.1b** is:

$\eta = \frac{U_p J_p}{P_0} \times 100\ \% = (4.64\ \pm\ 0.05)\ \%$

$FF = \frac{U_p J_p}{U_{os} J_{sc}} = 0.43 \ \pm \ 0.02$

The efficiency and fill factor calculation at 150 °C shown in **Fig. 4.1c** is:

$\eta = \frac{U_p J_p}{P_0} \times 100 \ \% = (4.24 \ \pm \ 0.19) \ \%$

$FF = \frac{U_p J_p}{U_{os} J_{sc}} = 0.43 \ \pm \ 0.02$

However, in our study, contrary to the aforementioned findings [79], we observed a consistent decrease in both efficiency and fill factor as the annealing temperature was increased.

4.1.2 Influence of FLA Energy Density on Si/PEDOT:PSS Solar Cell's Efficiency

In order to improve efficiency, we investigated FLA as an alternative post-treatment. Compared to traditional thermal annealing, FLA can lead to reduced thermal stress and offer the potential for fast thermal processing. The energy densities were carefully varied in order to discover the optimum conditions that would enhance the performance of the solar cell. After annealing, cells were electrically characterized to evaluate the impact of FLA energy densities on power conversion efficiency. The objective was to investigate if FLA could enhance the microstructural properties of the PEDOT:PSS film, thereby enhancing overall electrical properties and boosting the efficiency of the solar cell beyond what was achieved with conventional thermal annealing methods.

We expanded on existing literature [80], which identified 12 J/cm^2 as the optimal energy density for FLA of PEDOT:PSS/CZTS NC composites, by examining a broader range of energy densities in this experiment. It included energy densities of 8 J/cm^2 and 10 J/cm^{2}and 12 J/cm^2, increasing by 2 J/cm^2 step.

The efficiency and fill factor calculation at 8 J/cm^2 shown in **Fig. 4.2a** is:

$\eta = \frac{U_p J_p}{P_0} \times 100 \ \% = (3.77 \ \pm \ 0.06) \ \%$

$FF = \frac{U_p J_p}{U_{os} J_{sc}} = 0.42 \ \pm \ 0.02$

The efficiency and fill factor calculation at 10 J/cm^2 shown in **Fig. 4.2b** is:

$\eta = \frac{U_p J_p}{P_0} \times 100 \ \% = (3.03 \ \pm \ 0.46) \ \%$

$FF = \frac{U_p J_p}{U_{os} J_{sc}} = 0.38 \ \pm \ 0.03$

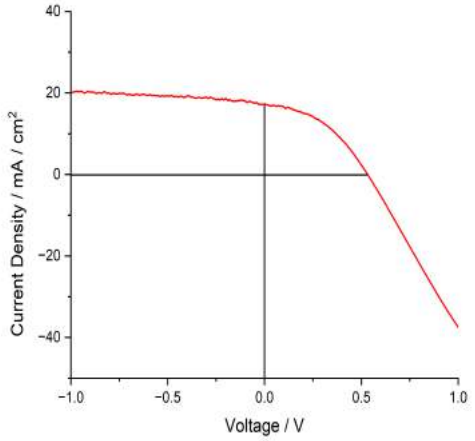

(a)

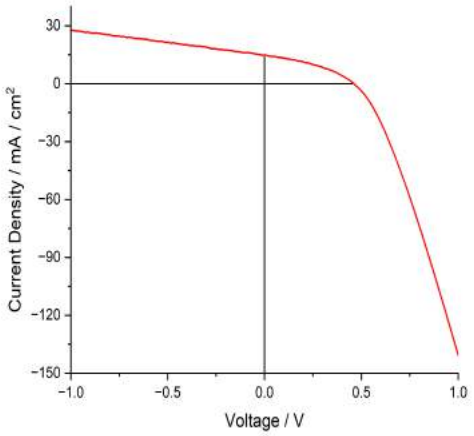

(b)

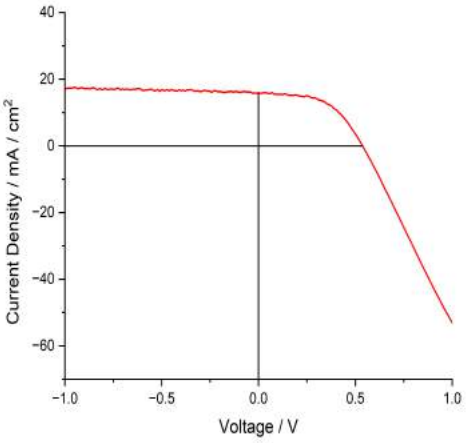

(c)

Figure 4.2: Illumination J-V characteristics for n-Si/PEDOT:PSS-solar cell treated by FLA energy density at (a) 8 J/cm² (b) 10 J/cm² and (c) 12 J/cm².

The efficiency and fill factor calculation at 12 J/cm² shown in **Fig. 4.2c** is:

$\eta = \frac{U_p J_p}{P_0} \times 100\ \% = (4.57\ \pm\ 0.05)\ \%$

$FF = \frac{U_p J_p}{U_{os} J_{sc}} = 0.54\ \pm\ 0.01$

The solar cells exhibited a 3.77 % efficiency with a fill factor of 0.42 at 8 J/cm² energy density of FLA. After increasing to 10 J/cm², the efficiency dropped to 3.03 % alongside a reduced fill factor of 0.38, suggesting that there could be a

limit beyond which the performance of the cell is adversely affected by the rise in energy density. Nonetheless, there was a noticeable increase in efficiency at 12 J/cm², reaching 4.57 % accompanied with a significantly higher fill factor of 0.54. This result not only supports prior literature findings [80] that a FLA treatment at 12 J/cm² was optimal for PEDOT:PSS/CZTS NC composites, but it also offers a particular efficiency baseline at this energy density.

The next expected step in our research, considering these results, was to go beyond the optimum level of 12 J/cm² that has previously been set for energy densities.The purpose of this research was to identify whether increasing energy densities would further enhance the PEDOT:PSS layer's electrical and microstructural characteristics , which could result in even higher efficiencies. Our next stage examined the effects of FLA at increased energy densities: 14 J/cm², 16 J/cm², and 18 J/cm² with a 2 J/cm² step increment.

The efficiency and fill factor calculation at 14 J/cm² shown in **Fig. 4.3a** is:

$\eta = \frac{U_p J_p}{P_0} \times 100\ \% = (5.09\ \pm\ 0.27)\ \%$

$FF = \frac{U_p J_p}{U_{os} J_{sc}} = 0.49\ \pm\ 0.02$

The efficiency and fill factor calculation at 16 J/cm² shown in **Fig. 4.3b** is:

$\eta = \frac{U_p J_p}{P_0} \times 100\ \% = (4.89\ \pm\ 0.48)\ \%$

$FF = \frac{U_p J_p}{U_{os} J_{sc}} = 0.46\ \pm\ 0.03$

The efficiency and fill factor calculation at 18 J/cm² shown in **Fig. 4.3c** is:

$\eta = \frac{U_p J_p}{P_0} \times 100\ \% = (5.05\ \pm\ 0.24)\ \%$

$FF = \frac{U_p J_p}{U_{os} J_{sc}} = 0.43\ \pm\ 0.03$

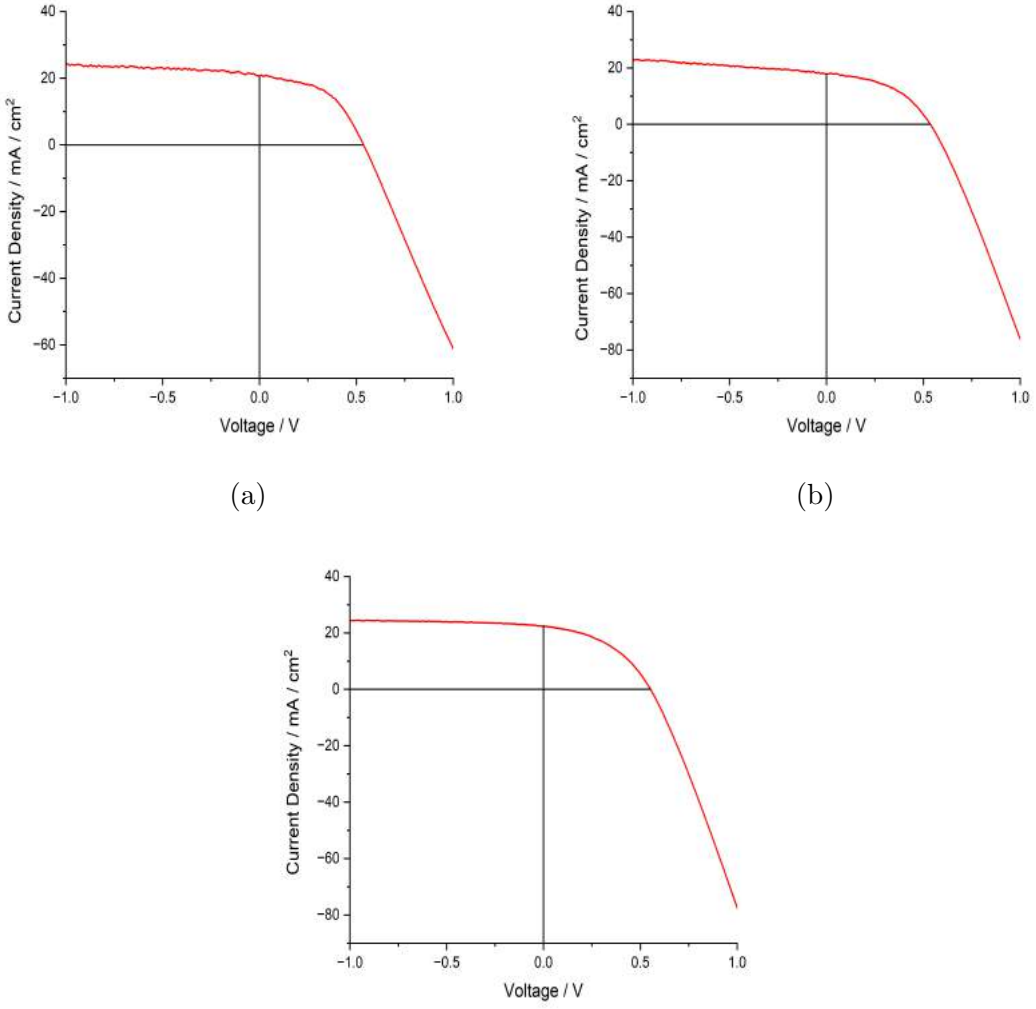

Figure 4.3: Illumination J-V characteristics for n-Si/PEDOT:PSS solar cell treated by FLA energy density at (a) 14 J/cm² (b) 16 J/cm² (c) 18 J/cm².

Exploring higher energy densities for PEDOT:PSS solar cells by FLA has produced informative results that show complex relationships between energy density, efficiency, and fill factor. The solar cells achieved an optimal efficiency of 5.09 % with an impressive fill factor of 0.49 at an energy density of 14 J/cm². In contrast, increasing the energy density to 16 J/cm² resulted in a slight decrease in efficiency to 4.89 %, alongside a fill factor reduction to 0.46. This pattern was maintained with a further increase to 18 J/cm², producing an efficiency of 5.05 % and a fill factor of 0.43. This gradual decline in performance at higher energy densities highlighted the possibility of thermal stress or structural damage.

Our findings indicated that 14 J/cm² is the optimal FLA energy density for our PEDOT:PSS solar cells, slightly higher than the 12 J/cm² recommended in the literature [80]. Higher FLA energy density increases polymer chain mobility and rearrangement, enhancing crystallinity and alignment for improved charge transport of PEDOT:PSS. This points out the necessity of modifying FLA conditions to suit the material composition and environment of the solar cell being developed.

Our research found that the optimum thermal annealing temperature for PEDOT:PSS solar cells is 75 °C, whereas the optimal energy density for FLA is 14 J/cm².

4.1.3 Raman Spectroscopy Evaluation of PEDOT:PSS Durability to High-Temperature Annealing and FLA Energy Densities

After we determined the optimal conditions for our PEDOT:PSS solar cell's thermal annealing and FLA, it was critical to find out how stable the material would be under rigorous conditions. The goal of this approach was to determine whether such intensive treatments could damage the structural integrity of the PEDOT:PSS material. The chemical composition and crystallinity of the samples after treatment were analyzed using Raman spectroscopy.

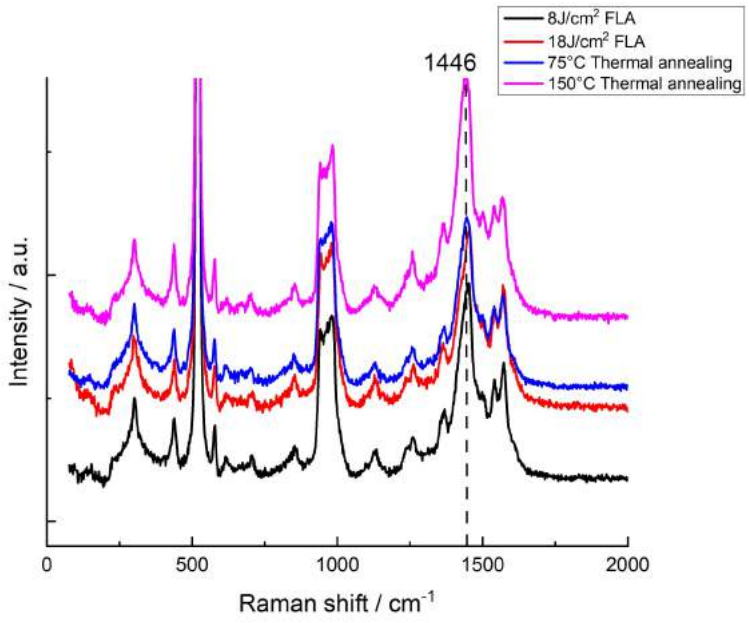

Figure 4.4: Set of Raman spectra for a PEDOT:PSS layer subjected to different post-deposition treatments.

The Raman shift, measured in cm^{-1}, indicates molecular vibrations within the material and is related to its structural properties. The Raman spectra showed in Fig. 4.4 that the peak at 1446 cm^{-1}, which corresponds to the C=C stretching in the PEDOT chain of PEDOT:PSS, varied significantly across samples with different treatments. Samples treated with 8 J/cm^2 FLA and 75 °C thermal annealing showed lower peak intensity at this wavenumber compared to those exposed to 18 J/cm^2 FLA, indicating changes in the material's structural order. The sample subjected to thermal annealing at 150 °C exhibited a significant increase in the peak intensity at 1446 cm^{-1}, indicating enhanced structural order or a phase transition resulting in increased Raman scattering within the material.

Based on these Raman spectroscopy results, the treatment conditions appear to impact the PEDOT:PSS structure. However, the structure appears to be modified rather than destroyed, as there is no degradation or complete disappearance of characteristic peaks. Higher energy densities and temperatures seem to change the molecule's structure, possibly resulting in increased crystallinity or other phase shifts rather than destruction.

4.2 Optimization of CZTS NCS Content in PEDOT:PSS Mixtures

In the next stage of my thesis experiment, I investigated the mixture of CZTS QDs with PEDOT:PSS by varying their volume percentage. The purpose of this experiment was to assess how the influence of varying concentrations of CZTS QDs within the PEDOT:PSS matrix could influence the solar cell's overall performance. This research was crucial for clarifying the complementary impacts of semiconductor QDs and conductive polymers, which will provide insights into developing more efficient solar cells.

These mixtures were immediately mixed by shaking and then deposited onto silicon substrates using a spin-coating process, as they were prone to "gelling" within an hour of preparation. After the completion of the "gelling" process, a clear differentiation between a transparent liquid and a solitary mass of black jelly was observed.

To begin, we added a small amount of 1 % CZTS to the PEDOT:PSS matrix and then gradually increased the quantity to 2 %, 3 %, and then 4 %. After the deposition process, these samples were subjected to thermal annealing at a precisely chosen temperature of 75 °C. The selection of this temperature was based on a previous investigation that identified it as the most optimal for enhancing the efficiency of PEDOT:PSS solar cells.

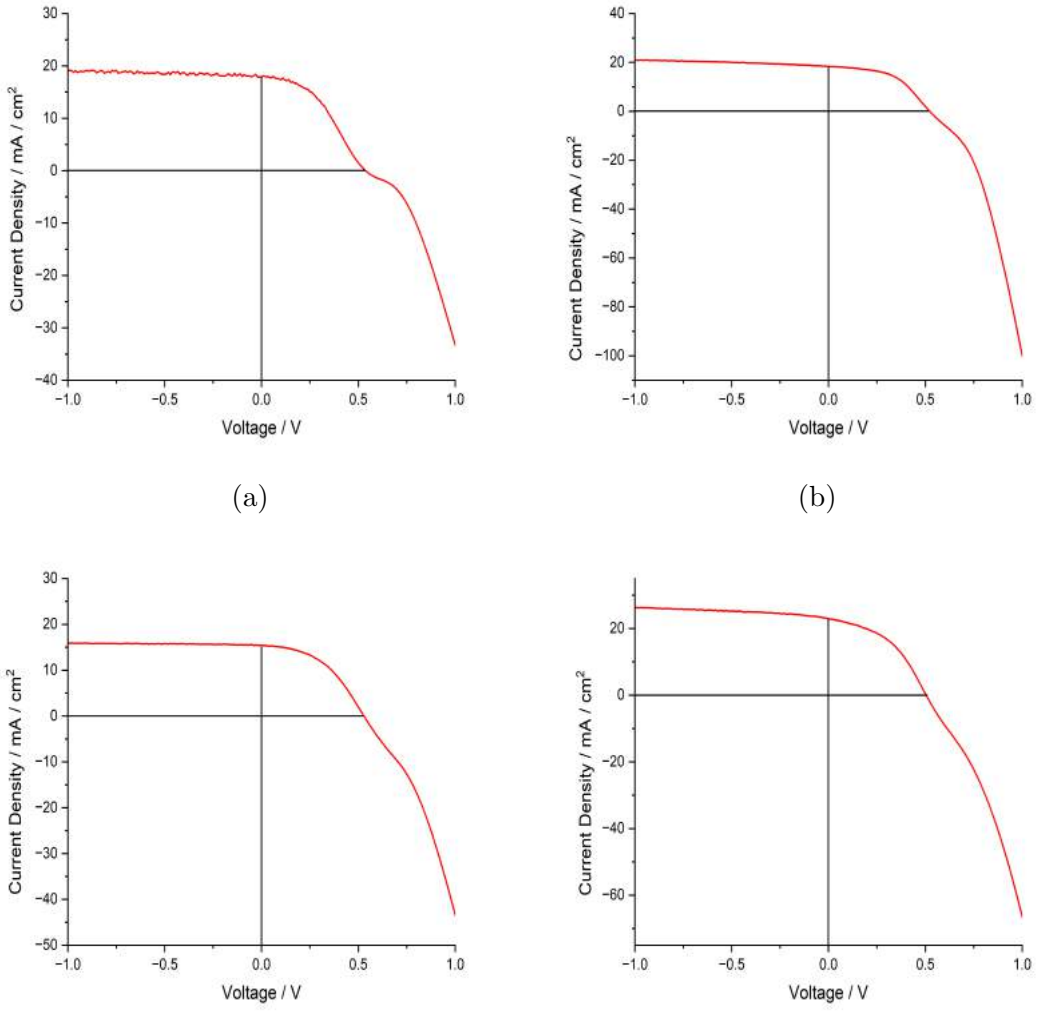

Figure 4.5: Illumination J-V characteristics for composite solar cells thermally annealed at 75 °C varying the concentration of CZTS and PEDOT:PSS (a) 1 % CZTS and 99 % PEDOT:PSS (b) 2 % CZTS and 98 % PEDOT:PSS (c) 3 % CZTS and 97 % PEDOT:PSS (d) 4 % CZTS and 96 % PEDOT:PSS.

The efficiency and fill factor calculation for 1 % CZTS and 99 % PEDOT:PSS shown in **Fig. 4.5a** is:

$$\eta = \frac{U_p J_p}{P_0} \times 100\ \% = (4.01\ \pm\ 0.12)\ \%$$

$$FF = \frac{U_p J_p}{U_{os} J_{sc}} = 0.41\ \pm\ 0.01$$

The efficiency and fill factor calculation for 2 % CZTS and 98 % PEDOT:PSS shown in **Fig. 4.5b** is:

$\eta = \frac{U_p J_p}{P_0} \times 100\ \% = (4.53\ \pm\ 0.29)\ \%$

$FF = \frac{U_p J_p}{U_{os} J_{sc}} = 0.45\ \pm\ 0.03$

The efficiency and fill factor calculation for 3 % CZTS and 97 % PEDOT:PSS shown in **Fig. 4.5c** is:

$\eta = \frac{U_p J_p}{P_0} \times 100\ \% = (3.40\ \pm\ 0.29)\ \%$

$FF = \frac{U_p J_p}{U_{os} J_{sc}} = 0.46\ \pm\ 0.02$

The efficiency and fill factor calculation for 4 % CZTS and 96 % PEDOT:PSS shown in **Fig. 4.5d** is:

$\eta = \frac{U_p J_p}{P_0} \times 100\ \% = (5.06\ \pm\ 0.04)\ \%$

$FF = \frac{U_p J_p}{U_{os} J_{sc}} = 0.44\ \pm\ 0.01$

Adding various amounts of CZTS to PEDOT:PSS solar cells has distinct effects on their efficiency and fill factor, revealing a non-linear relationship between CZTS concentration and solar cell performance. When 1 vol. % of CZTS was added to PEDOT:PSS, the solar cell exhibited an efficiency of 4.01 % and a fill factor of 0.41. These results established a foundation for evaluating the impact of CZTS incorporation. On increasing the CZTS volume percentage to 2 %, a significant improvement was observed in both efficiency, reaching 4.53 %, and fill factor, which reached its peak at 0.5. It seemed that at this concentration, CZTS has a positive impact on the solar cell's performance, possibly because of improved absorption and charge carrier pathways.

However, further increasing the CZTS to 3 % resulted in a decline in efficiency to 3.4 % and a slight drop in the fill factor to 0.46. It was surprising that at 4 % CZTS, the efficiency went up a lot to 5.06 %, but the fill factor went down a little to 0.44 compared to the 2 % CZTS sample. This improvement in efficiency might be attributed to a threshold concentration of CZTS that facilitated better light harvesting or charge separation, outweighing the negative impacts on the fill factor.

The results of our studies indicate the complex correlation between the concentration of CZTS and the efficiency of PEDOT:PSS solar cells. These results show that adding CZTS up to a certain point can make the solar cells more efficient and increase their fill factor. Nevertheless, adding too much CZTS might make them

less efficient. Understanding this delicate balance means that finding the optimal CZTS concentration is critical for achieving the best solar cell performance.

With this fundamental understanding, we were motivated to explore deeper into the impacts of CZTS on the efficiency of solar cells by expanding our research to higher concentrations of CZTS. In the following set of experiments, we gradually increased the quantity of CZTS to 5 %, 6 %, and 7 %. This step focused on identifying the optimal CZTS concentration to maximize PEDOT:PSS-CZTS solar cell efficiency.

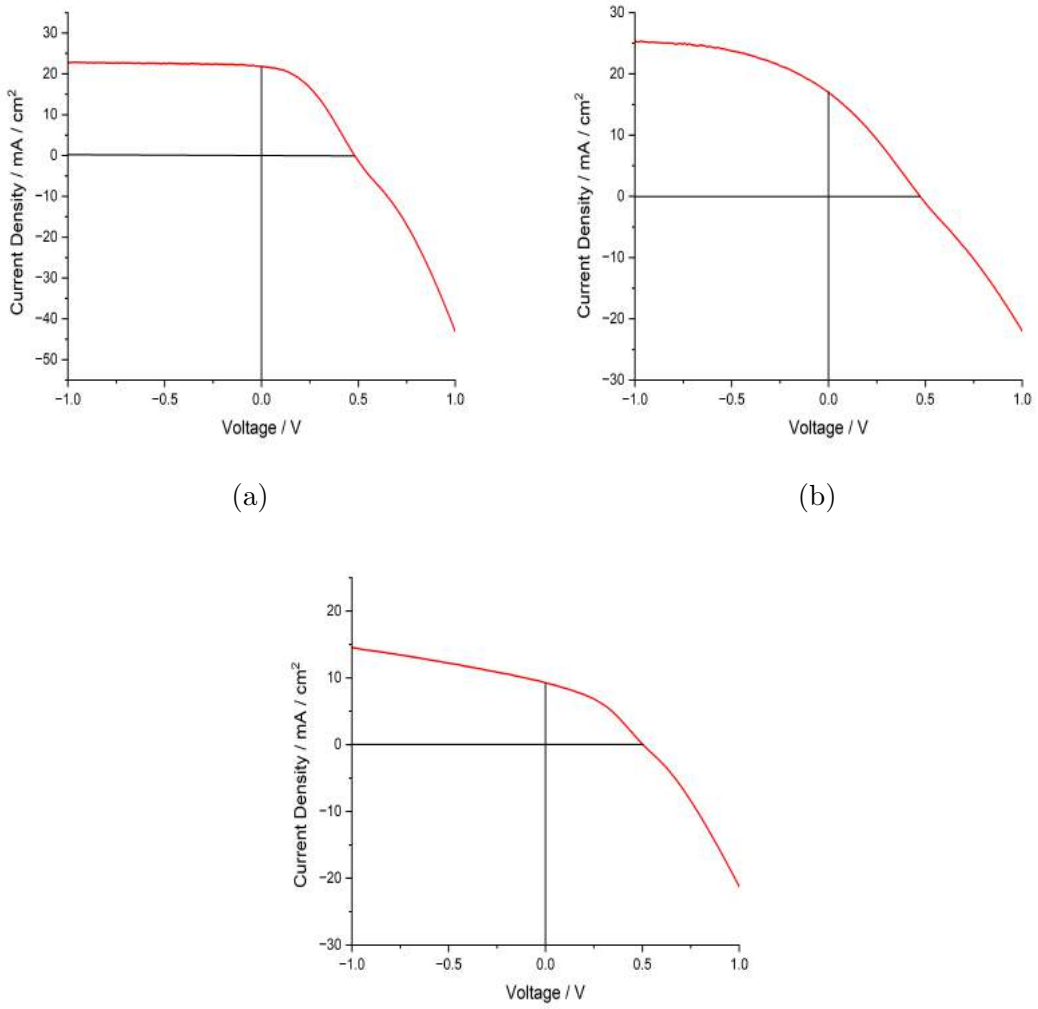

Figure 4.6: Illumination J-V characteristics for composite solar cells thermally annealed at 75 °C varying the concentration of CZTS and PEDOT:PSS (a) 5 % CZTS and 95 % PEDOT:PSS (b) 6 % CZTS and 94 % PEDOT:PSS (c) 7 % CZTS and 93 % PEDOT:PSS.

The efficiency and fill factor calculation for 5 % CZTS and 95 % PEDOT:PSS shown in **Fig. 4.6a** is:

$\eta = \frac{U_p J_p}{P_0} \times 100\ \% = (4.21\ \pm\ 0.60)\ \%$

$FF = \frac{U_p J_p}{U_{os} J_{sc}} = 0.40\ \pm\ 0.01$

The efficiency and fill factor calculation for 6 % CZTS and 94 % PEDOT:PSS shown in **Fig. 4.6b** is:

$\eta = \frac{U_p J_p}{P_0} \times 100\ \% = (2.11\ \pm\ 0.2)\ \%$

$FF = \frac{U_p J_p}{U_{os} J_{sc}} = 0.29\ \pm\ 0.01$

The efficiency and fill factor calculation for 7 % CZTS and 93 % PEDOT:PSS shown in **Fig. 4.6c** is:

$\eta = \frac{U_p J_p}{P_0} \times 100\ \% = (1.93\ \pm\ 0.14)\ \%$

$FF = \frac{U_p J_p}{U_{os} J_{sc}} = 0.39\ \pm\ 0.02$

The experiments we conducted with different concentrations of CZTS in PEDOT:PSS solar cells has helped us determine the optimal CZTS ratio to improve solar cell performance. With a CZTS volume percentage of 5 %, the solar cells demonstrated an efficiency of 4.21 % and a fill factor of 0.40, indicating that they are approaching the threshold of ideal performance. Nevertheless, when the CZTS concentration was further raised to 6 %, a notable decrease in efficiency to 2.11 % was found, accompanied with a lower fill factor of 0.29. A significant decline in performance corresponded with a noticeable physical incident: the PEDOT:PSS/CZTS mixture began to agglomerate rapidly, leading to gelling. This gelling effect occurred even when the solution was freshly mixed before deposition. This led to non-homogeneous deposition, which adversely affected the uniformity and, eventually, the effectiveness of the solar cells.

Continuing the pattern, the efficiency of the CZTS concentration at 7 % declined to 1.93 %, while the fill factor had a little increase to 0.39. The observed rise in fill factor, however peculiar, does not compensate for the substantial drop in efficiency. This decline can be attributed to the degraded morphological quality of the film caused by the previously mentioned issues of gelling and agglomeration.

Upon conducting a thorough analysis, it was evident that concentrations of CZTS over 5% had a negative effect on the performance of the solar cell. This is directly attributed to the material's instability and difficulties in processing. The phenomenon of gelation, which occurs at higher concentrations, hinders the uniformity of the

film, which is a crucial factor of solar cell efficiency.

Therefore, we concluded that a CZTS concentration of 4 % is the most optimal for PEDOT:PSS-CZTS solar cells. This concentration not only avoids the agglomeration issues experienced at higher percentages, but also establishes an overall balance between efficiency and fill factor.

4.3 Optimizing Post-Treatment Parameters for Si/PEDOT:PSS-CZTS Composite Solar Cell

This study focused on optimizing the post-treatment parameters for a hybrid solar cell composed of Si/PEDOT:PSS-CZTS composites. Through the process of refining these parameters, our objective was to improve the efficiency and stability of the solar cell's performance.

4.3.1 Optimization of Thermal Annealing Temperature for Si/PEDOT:PSS-CZTS Composite Solar Cell

In this step, our objective was to investigate if the previously determined optimal thermal annealing temperature of 75 °C for pure PEDOT:PSS solar cells remained true for CZTS-incorporated PEDOT:PSS solar cells. The addition of CZTS to the PEDOT:PSS may cause a change in the optimum annealing conditions, due to the interactions between PEDOT:PSS and CZTS. In order to confirm this, our strategy involved raising the thermal annealing temperature to 100 °C for the PEDOT:PSS-CZTS composite solar cells.

The efficiency and fill factor calculation for 4 % CZTS and 96 % PEDOT:PSS shown in **Fig. 4.7** is:

$$\eta = \frac{U_p J_p}{P_0} \times 100\ \% = (3.64\ \pm\ 0.90)\ \%$$

$$FF = \frac{U_p J_p}{U_{os} J_{sc}} = 0.35\ \pm\ 0.02$$

When we increased the thermal annealing temperature to 100 °C for the PEDOT:PSS-CZTS solar cells, we saw a significant decline in performance. The efficiency decreased to 3.64 % and the fill factor dropped to 0.35. In contrast, our observed results showed that annealing the PEDOT:PSS-CZTS solar cells to 75 °C led to much higher efficiency level (5.06 %) and fill factor (0.44). The comparison of these results clearly showed that the optimum temperature for thermal annealing for PEDOT:PSS-CZTS solar cells is 75 °C, which is the same temperature as for

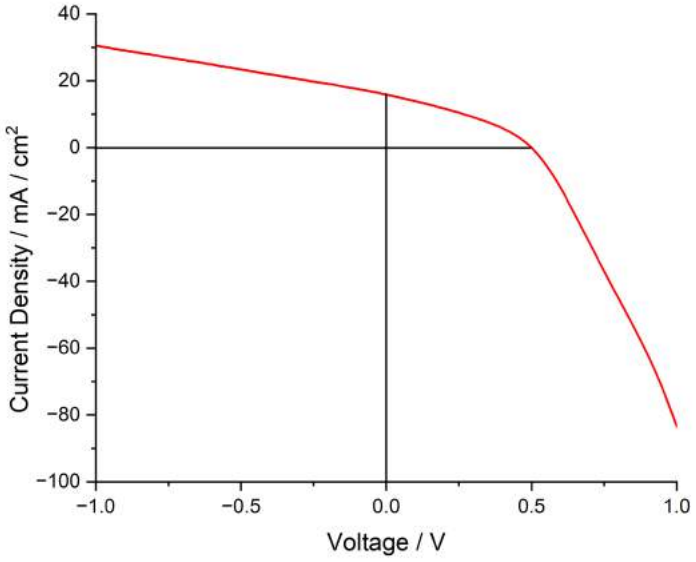

Figure 4.7: Illumination J-V characteristics for composite solar cells thermally annealed at 100 °C with the concentration of 4 % CZTS and 96 % PEDOT:PSS.

pure PEDOT:PSS solar cells.

It's clear that the annealing temperature has an enormous impact on the PV performance of composite solar cells. In order to obtain optimal results out of the efficiency and fill factor of PEDOT:PSS-CZTS solar cells, the annealing temperature must be kept at 75 °C.

4.3.2 Influence of FLA Energy Density on Si/PEDOT:PSS-CZTS Composite Solar Cell's Efficiency

In our continuous efforts to improve the efficiency of PEDOT:PSS-CZTS solar cells, we did an experiment to find out how different energy densities of FLA affect their performance. The experiment was started with an energy density of 12 J/cm^2, which corresponds to the recommended value found in the literature for identical composite materials [80]. The initial choice was made intentionally to determine if the energy density of our PEDOT:PSS-CZTS composition aligns with existing standards.

According to our results, we have demonstrated that the optimum energy density for pure PEDOT:PSS solar cells is 14 J/cm^2. We were interested to examine if adding CZTS would require a change in this value. In order to achieve this objec-

tive, we initiated the FLA treatment at an energy density of 12 J/cm². We then increased the energy density in gradual steps, observing the results at 14 J/cm² and subsequently at 16 J/cm².

The primary objective of this experiment was to ascertain whether the optimum FLA energy density for PEDOT:PSS-CZTS cells matched the recommendations found in existing literature [80], correspond to the optimal value for pure PEDOT:PSS, or reveal a completely new optimal value.

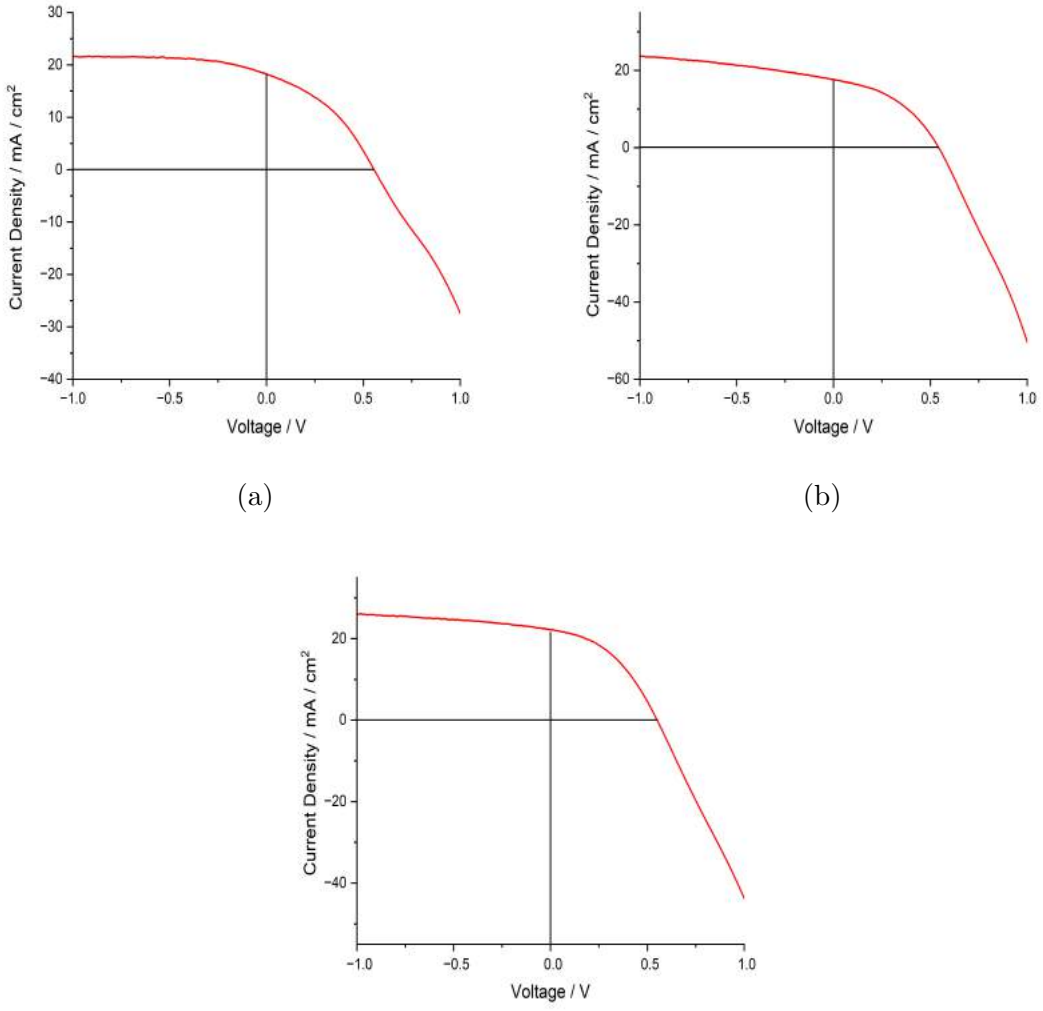

Figure 4.8: Illumination J-V characteristics for composite solar cells with the concentration of 4 % CZTS and 96 % PEDOT:PSS treated by FLA energy density at (a) 12 J/cm² (b) 14 J/cm² and (c) 16 J/cm².

The efficiency and fill factor calculation at 12 J/cm² shown in **Fig. 4.8a** is:

$\eta = \frac{U_p J_p}{P_0} \times 100\ \% = (3.23\ \pm\ 0.62)\ \%$

$FF = \frac{U_p J_p}{U_{os} J_{sc}} = 0.38\ \pm\ 0.02$

The efficiency and fill factor calculation at 14 J/cm^2 shown in **Fig. 4.8b** is:

$\eta = \frac{U_p J_p}{P_0} \times 100\ \% = (3.68\ \pm\ 0.28)\ \%$

$FF = \frac{U_p J_p}{U_{os} J_{sc}} = 0.41\ \pm\ 0.01$

The efficiency and fill factor calculation at 16 J/cm^2 shown in **Fig. 4.8c** is:

$\eta = \frac{U_p J_p}{P_0} \times 100\ \% = (5.11\ \pm\ 0.02)\ \%$

$FF = \frac{U_p J_p}{U_{os} J_{sc}} = 0.42\ \pm\ 0.01$

Results from our experiment investigating the influence of FLA energy density on the performance of PEDOT:PSS-CZTS solar cells demonstrated a noticeable trend of improved efficiency and fill factor as the energy density increases. Starting at value of 12 J/cm^2, the efficiency was calculated to be 3.23 %, and the fill factor was 0.38. By increasing the FLA energy density to 14 J/cm^2, the efficiency and fill factor both went up to 3.68 % and 0.41, respectively. The most significant enhancement was noticed at an energy density of 16 J/cm^2, resulting in an efficiency increase of 5.11 % and a fill factor of 0.42.

These findings are particularly notable when compared to both the literature and the results from our previous experiments with pure PEDOT:PSS solar cells. The literature suggested an optimal FLA energy density of 12 J/cm^2 for similar composite materials [80], at which we observed the lowest efficiency in our current series. In our previous experiments, we found that 14 J/cm^2 was the optimal energy density for pure PEDOT:PSS cells. However, for PEDOT:PSS-CZTS solar cells, we observed higher efficiency at 16 J/cm^2.

These new findings suggested that for PEDOT:PSS-CZTS composites, higher FLA energy densities may be preferable. Consequently, in the following phase of experiment, we chose to increase the FLA energy density to 17 J/cm^2 and 18 J/cm^2. Additionally, to refine our understanding and pinpoint the precise optimum, we introduced variations by testing at 15 J/cm^2.

The efficiency and fill factor calculation at 15 J/cm^2 shown in **Fig. 4.9a** is:

$\eta = \frac{U_p J_p}{P_0} \times 100\ \% = (4.05\ \pm\ 0.21)\ \%$

$FF = \frac{U_p J_p}{U_{os} J_{sc}} = 0.42\ \pm\ 0.02$

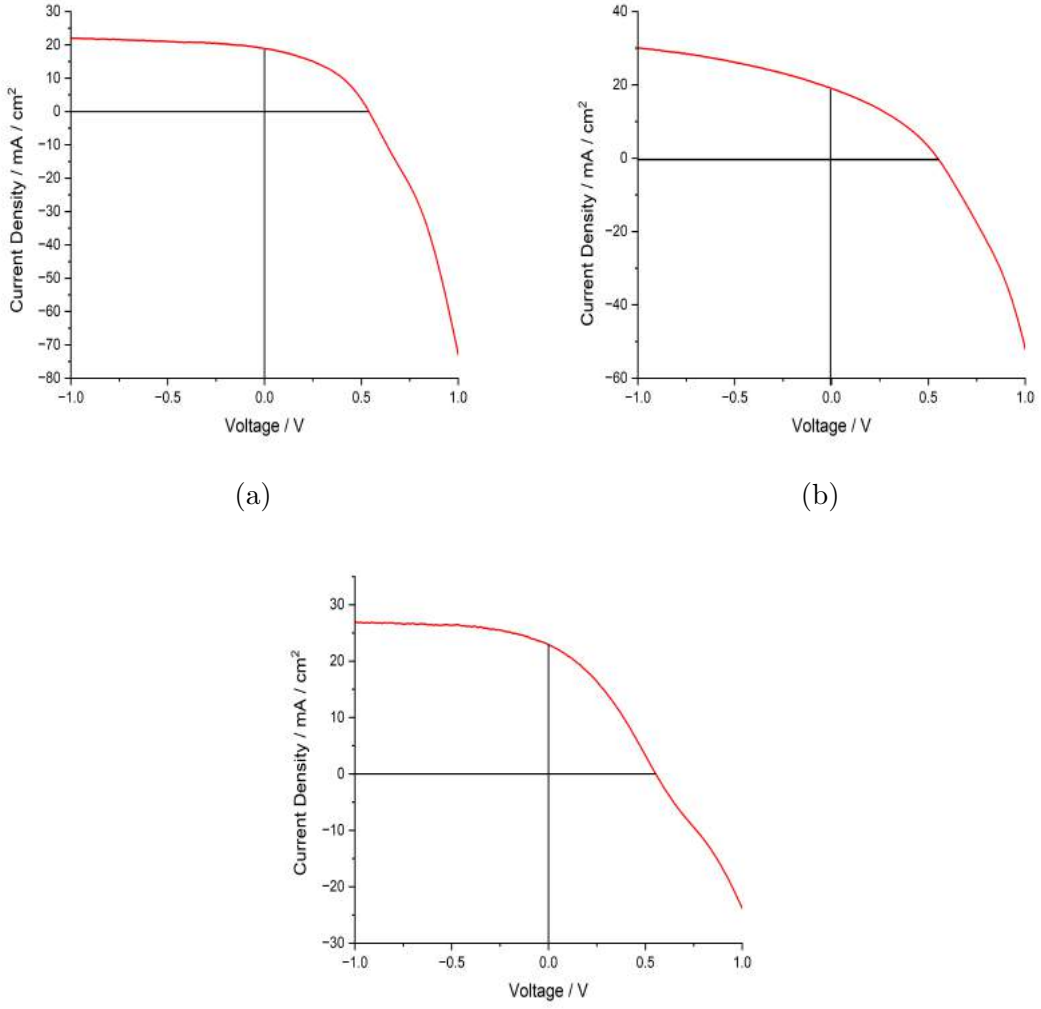

Figure 4.9: Illumination J-V characteristics for composite solar cells with the concentration of 4 % CZTS and 96 % PEDOT:PSS treated by FLA energy density at (a) 15 J/cm² (b) 17 J/cm² and (c) 18 J/cm².

The efficiency and fill factor calculation at 17 J/cm² shown in **Fig. 4.9b** is:

$\eta = \frac{U_p J_p}{P_0} \times 100\ \% = (4.19\ \pm\ 0.64)\ \%$

$FF = \frac{U_p J_p}{U_{os} J_{sc}} = 0.34\ \pm\ 0.02$

The efficiency and fill factor calculation at 18 J/cm² shown in **Fig. 4.9c** is:

$\eta = \frac{U_p J_p}{P_0} \times 100\ \% = (4.07\ \pm\ 0.22)\ \%$

$FF = \frac{U_p J_p}{U_{os} J_{sc}} = 0.34\ \pm\ 0.01$

This in-depth study of PEDOT:PSS-CZTS solar cells exposed to different FLA energy densities has led to interesting findings , further refining our understanding of optimal fabrication parameters. With a FLA energy density of 15 J/cm^2, the solar cells showed an efficiency of 4.05 % and a fill factor of 0.42. When the energy level was raised to 17 J/cm^2, there was a small rise in efficiency to 4.19 %, but the fill factor dropped to 0.34 at the same time. When the energy density was raised even more to 18 J/cm^2, the efficiency went down a little to 4.07 %, but the fill factor stayed the same at 0.34.

The comparison of findings from multiple experiments has conclusively shown that an energy density of 16 J/cm^2 is the most effective for FLA in PEDOT:PSS-CZTS solar cells. This energy density has resulted in a notable efficiency of 5.11 % and a fill factor of 0.42. This optimal energy density not only correlates to the optimum level of performance found in the current experiments, but also demonstrates a significant enhancement in efficiency and the ability to maintain a high fill factor compared to other evaluated energy densities.

Our thorough analysis of the FLA and thermal annealing processes across several sets of experiments enabled us to make significant findings about the fabrication of PEDOT:PSS and PEDOT:PSS-CZTS solar cells. The optimum energy density of FLA, identified as 16 J/cm^2, indeed facilitated higher efficiency in both pure PEDOT:PSS and PEDOT:PSS-CZTS solar cells compared to the optimum thermal annealing temperature, identified as 75 °C. The FLA process, especially when it used the right amount of energy density, seems to alter the characteristics of the material more favorably than thermal annealing. This can lead to better charge carrier movement, better light absorption, or reduced defect densities.

Furthermore, it can be said that the integration of CZTS into PEDOT:PSS solar cells significantly enhances their efficiency compared to cells composed solely of pure PEDOT:PSS. This improvement is observed following both thermal annealing and FLA treatments.

4.4 Innovating PEDOT:PSS/CZTS Solar Cell Production: A Dual Approach with Spray and Spin Coating to Overcome Material Complications

Our next experiment used an advanced approach that combined spin and spray coating processes in an effort to improve the manufacturing procedures for PEDOT:PSS solar cells integrated with CZTS. The major goal of this experiment was to investigate the effect of layer-by-layer material fabrication on solar cell efficiency when compared to mixed composite solar cells. This method included depositing individual material layers sequentially, rather than combining all materials into a single composite mixture for deposition. The mixed material of PEDOT:PSS and CZTS was denoted as PEDOT:PSS-CZTS, while layers of PEDOT:PSS and CZTS are denoted as PEDOT:PSS/CZTS.

4.4.1 Evaluating Thermal Annealing's Impact on Layered PEDOT:PSS/CZTS Solar Performance

The experiment began by carefully preparing the CZTS solution. Initially, a concentrated CZTS solution was diluted tenfold by mixing 9 mL of deionized water to 1 mL of the concentrated solution. The diluted solution was coated on the substrate using a spray coating device, with particular emphasis on obtaining the desired thickness of the layer. In order to achieve uniformity and sufficient coverage, the cycle iteration for the spray deposition was carefully varied. The process parameters were controlled, maintaining a constant temperature of 90 °C to facilitate solvent evaporation and film formation, a nozzle speed of 2 mm/s to ensure steady deposition, and a minimum nozzle height of 3.8 cm to optimize the spray coverage area.

Following the successful deposition of the CZTS layer, the next step involved applying the PEDOT:PSS layer. Due to the observed tendency of the PEDOT:PSS/CZTS mixture to agglomerate, which posed a significant risk of clogging the spray nozzle, spin coating was chosen as an alternate approach for PEDOT:PSS deposition.

Following the successful layer deposition, the solar cells were thermally annealed at 75 °C, which has been found to be the optimal temperature for PEDOT:PSS/CZTS solar cells. The thermal treatment was necessary to improve the interfacial adhesion between the CZTS and PEDOT:PSS layers, in addition to enhance the crystallinity and electrical properties of the materials.

In the first phase of our experiment on layer-by-layer solar cell preparation, we varied the spraying cycles for the CZTS layer to optimize its thickness. Starting with

5 cycles, we gradually increased to 7 and then to 10 cycles. We next deposited a layer of PEDOT:PSS by spin coating. The constructed solar cells were then thermally annealed at 75 °C and subsequently electrically characterized using a solar simulator.

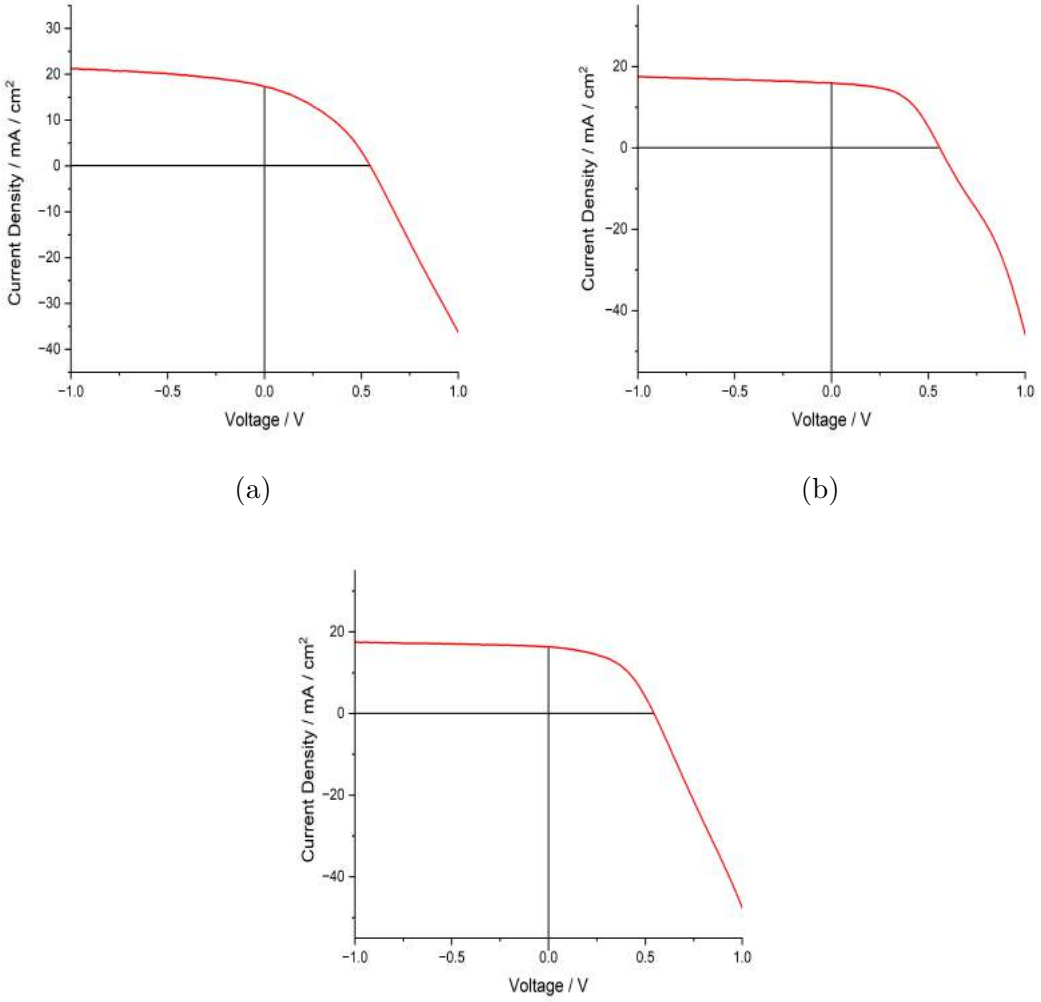

Figure 4.10: Illumination J-V Characteristics for n-Si/CZTS (Spray Coating)/ PEDOT:PSS (Spin Coating) solar cells thermally annealed at 75 °C with (a) 5 Spraying Cycles of CZTS (b) 7 Spraying Cycles of CZTS and (c) 10 Spraying Cycles CZTS.

The efficiency and fill factor calculation at 5 Spraying Cycles of CZTS shown in **Fig. 4.10a** is:

$\eta = \frac{U_p J_p}{P_0} \times 100\ \% = (3.46\ \pm\ 0.12)\ \%$

$FF = \frac{U_p J_p}{U_{os} J_{sc}} = 0.38 \ \pm \ 0.02$

The efficiency and fill factor calculation at 7 Spraying Cycles of CZTS shown in **Fig. 4.10b** is:

$\eta = \frac{U_p J_p}{P_0} \times 100 \ \% = (4.47 \ \pm \ 0.20) \ \%$

$FF = \frac{U_p J_p}{U_{os} J_{sc}} = 0.53 \ \pm \ 0.03$

The efficiency and fill factor calculation at 10 Spraying Cycles of CZTS shown in **Fig. 4.10c** is:

$\eta = \frac{U_p J_p}{P_0} \times 100 \ \% = (4.22 \ \pm \ 0.15) \ \%$

$FF = \frac{U_p J_p}{U_{os} J_{sc}} = 0.49 \ \pm \ 0.01$

Our layer-by-layer deposition experiment of PEDOT:PSS/CZTS solar cells, followed by thermal annealing at 75 °C, provided comprehensive understanding of the impact of spraying cycles on solar cell performance. At a baseline of 5 spraying cycles, the efficiency was 3.46 %, with a fill factor of 0.38. Increasing the spraying cycles to 7 significantly increased efficiency to 4.47 %, with a noteworthy fill factor of 0.53. However, increasing the number of spraying cycles to 10 resulted in a minor decreased in efficiency to 4.22 % while maintaining a relatively high fill factor of 0.49.

From these comparisons of findings, it was evident that the 7 spraying cycle provided the optimum performance in terms of efficiency and fill factor. The increase in spraying cycles from 5 to 7 seemed to enhance the structural and electrical properties of solar cells, leading to improved performance. However, the following increase to 10 cycles, while still showing greater efficiency than the 5-cycle deposition, indicated a declining return. This could be due to the film's growing thickness at this stage, which hinders charge carrier movement and increases recombination, reducing overall efficiency.

The layer-by-layer method at 7 spraying cycles exhibited slightly lower efficiency when compared to the efficiency of the composite mixture PEDOT:PSS/CZTS solar cells, which achieved an efficiency of 5.06 % and a fill factor of 0.44.

4.4.2 Investigating the Influence of FLA on Layered PEDOT:PSS/CZTS Solar Cells Performance

In our next experiment, we investigated the impact of FLA on PEDOT:PSS/CZTS solar cells that were produced layer by layer. We used a FLA energy density of 16 J/cm^2, which was previously identified as optimal. In order to compare the impact of FLA and thermal annealing on the efficiency of solar cells, we modified the spraying cycles at 5, 7, and 10,using the same techniques as previously.

The goal of this experiment was to find out the specific impacts of FLA and thermal annealing on the PV efficiency of solar cells constructed using a layer-by-layer method.

The efficiency and fill factor calculation at 5 Spraying Cycles of CZTS ahown in **Fig. 4.11a** is:

$\eta = \frac{U_p J_p}{P_0} \times 100\ \% = (5.17\ \pm\ 0.26)\ \%$

$FF = \frac{U_p J_p}{U_{os} J_{sc}} = 0.47\ \pm\ 0.02$

The efficiency and fill factor calculation at 7 Spraying Cycles of CZTS ahown in **Fig. 4.11b** is:

$\eta = \frac{U_p J_p}{P_0} \times 100\ \% = (5.52\ \pm\ 0.24)\ \%$

$FF = \frac{U_p J_p}{U_{os} J_{sc}} = 0.51\ \pm\ 0.02$

The efficiency and fill factor calculation at 10 Spraying Cycles of CZTS ahown in **Fig. 4.11c** is:

$\eta = \frac{U_p J_p}{P_0} \times 100\ \% = (4.45\ \pm\ 0.2)\ \%$

$FF = \frac{U_p J_p}{U_{os} J_{sc}} = 0.43\ \pm\ 0.01$

After conducting our experiment, which examined the effects of FLA on PEDOT:PSS/CZTS solar cells, we achieved significant results using an optimum FLA energy density of 16 J/cm^2, throughout several spraying cycles. After 5 spraying cycles, the solar cells achieved an efficiency of 5.17 % and a fill factor of 0.47. Increasing the spraying cycles to 7 increased efficiency and fill factor to 5.52 % and 0.51, respectively. However, increasing the number of spraying cycles to 10 led to a decreased in efficiency to 4.45 %, with the fill factor also dropping to 0.43.

Comparing these outcomes, it is evident that 7 spraying cycles yield the maximum efficiency and fill factor, suggesting optimal layer thickness and uniformity for solar

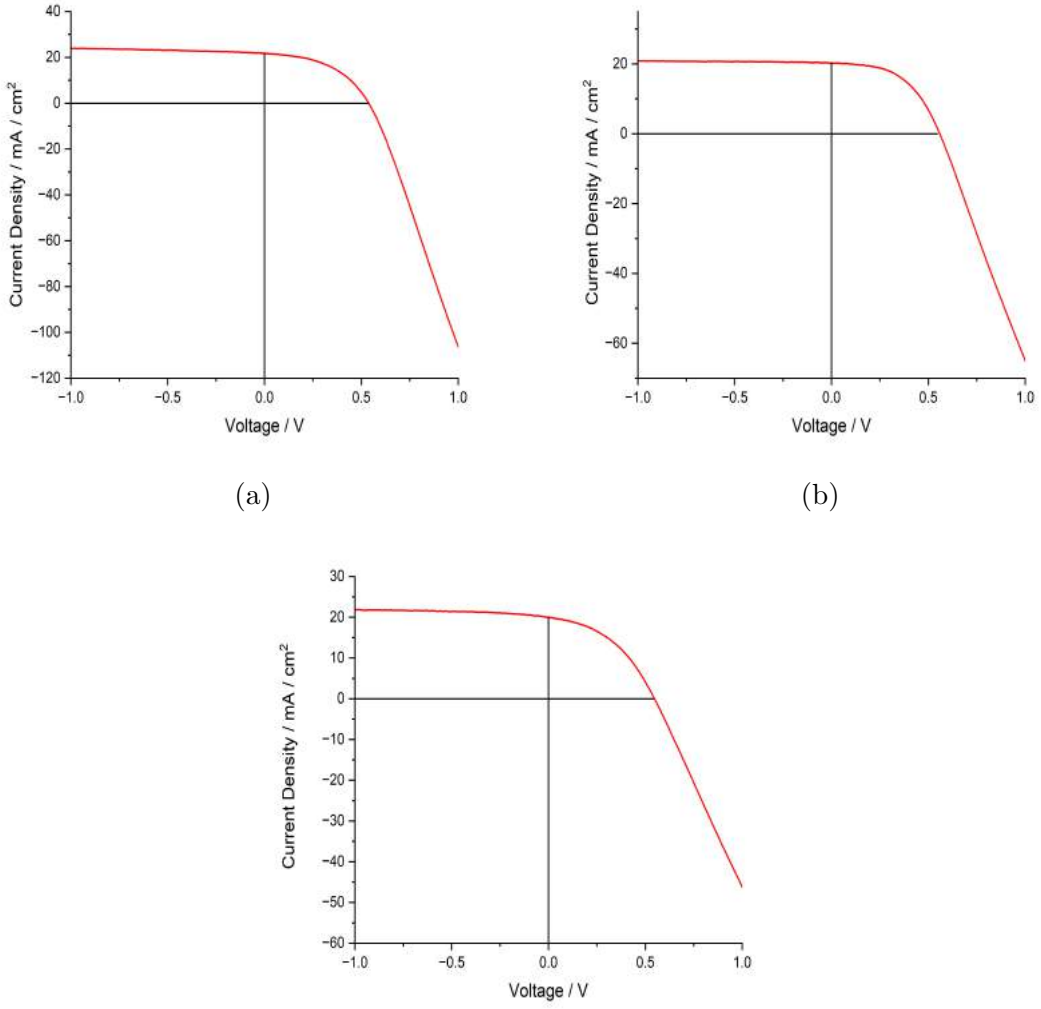

Figure 4.11: Illumination J-V Characteristics for n-Si/CZTS (Spray Coating)/ PEDOT:PSS (Spin Coating) solar cells FLA energy density at 16 J/cm^2 with (a) 5 spraying cycles of CZTS (b) 7 spraying cycles of CZTS and (c) 10 spraying cycles CZTS.

cell performance. In contrast to our previous thermal annealing findings, which showed an optimal efficiency of 4.47 % and a fill factor of 0.53 at 75 °C, the FLA method at 7 spraying cycles demonstrated superior efficiency. This comparison shows that, while thermal annealing produces a high fill factor, FLA at an optimal spraying cycle and energy density can achieve higher efficiency. This implies that FLA can enhance layer-by-layer PEDOT:PSS/CZTS solar cell performance better than thermal annealing, indicating its potential for enhancing advanced solar cell photovoltaic efficiency.

The layer-by-layer PEDOT:PSS/CZTS solar cells, with 7 spraying cycles and treated with FLA at 16 J/cm², achieved a higher efficiency of 5.52 % and fill factor of 0.51 compared to mixed composite PEDOT:PSS/CZTS cells at the same FLA conditions, which had an efficiency of 5.11 % and a fill factor of 0.42.

4.4.3 Investigating the Impact of Double-Layered CZTS and PEDOT:PSS Configurations on Solar Cell Efficiency

In the next experiment, we investigated the impact of fabricating solar cells with two layers each of CZTS and PEDOT:PSS on their efficiency. First, we used spray coating to deposit a layer of CZTS, and then spin coating to deposit a layer of PEDOT:PSS. Then, using spin coating once more, a second layer of CZTS was applied. Finally, a coating of PEDOT:PSS was applied on the top using the spin coating technique. The purpose of this dual-layer structure was to investigate possible synergistic effects on solar cell performance, especially with respect to efficiency.

After stacking, the solar cells were exposed to 16 J/cm² FLA, which was proven to yield a higher efficiency than optimum thermal annealing for our materials. To fully examine the impact of this dual-layer technique, we varied the spraying cycles for the initial CZTS layer, beginning with 5 and gradually increasing to 7. This variation tried to identify the best thickness and coverage that would enhance the PV efficiency of the solar cells.

The goal of this experiment was to examine the effect of adding a second layer of both CZTS and PEDOT:PSS on the solar cells over performance.

The efficiency and fill factor calculation at 5 spraying cycles of CZTS shown in **Fig. 4.12a**:

$$\eta = \frac{U_p J_p}{P_0} \times 100\ \% = (4.01\ \pm\ 0.20)\ \%$$

$$FF = \frac{U_p J_p}{U_{os} J_{sc}} = 0.43\ \pm\ 0.03$$

The efficiency and fill factor calculation at 7 spraying cycles of CZTS shown in **Fig. 4.12b** is:

$$\eta = \frac{U_p J_p}{P_0} \times 100\ \% = (3.93\ \pm\ 0.21)\ \%$$

$$FF = \frac{U_p J_p}{U_{os} J_{sc}} = 0.54\ \pm\ 0.03$$

Our experiments with double-layered CZTS and PEDOT:PSS on solar cells treated with FLA at 16 J/cm² revealed interesting trends in efficiency and fill factor throughout spraying cycles. The efficiency for the configuration with 5 spraying cycles was

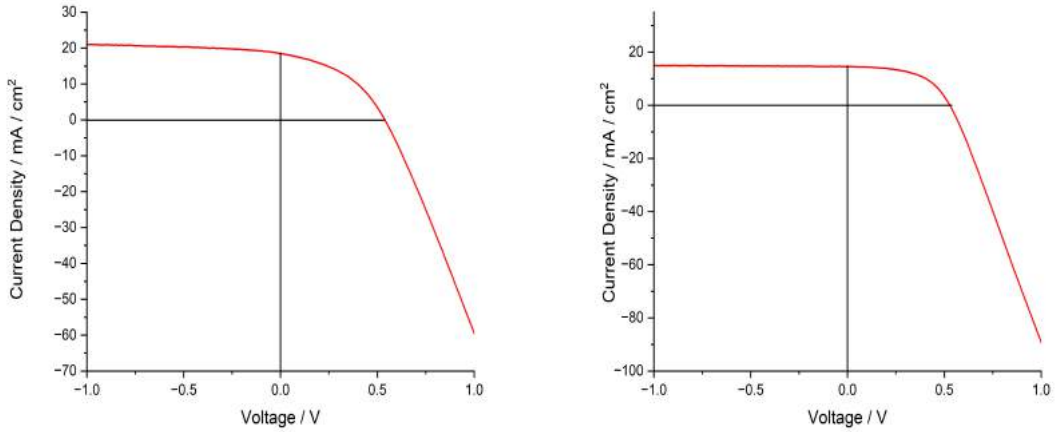

(a) (b)

Figure 4.12: Illumination J-V Characteristics for n-Si/CZTS (Spray Coating)/ PEDOT:PSS (Spin Coating)/CZTS (spin coating)/PEDOT:PSS (spin coating) double layered solar cells FLA energy density at 16 J/cm² with (a) 5 spraying cycles of CZTS and (b) 7 spraying cycles of CZTS.

4.01 %, with a fill factor of 0.43. When the number of spraying cycles was raised to 7, efficiency decreased a bit to 3.93 %, but with an improved fill factor of 0.54.

When compared to the results from the single layer-by-layer structure, where the optimal setup achieved an efficiency of 5.52 % with a fill factor of 0.51 after 7 spraying cycles, the double-layered strategy appears to be less efficient. While the single layer-by-layer method achieved a higher efficiency, the double-layer structure, particularly at 7 spraying cycles, has a higher fill factor.

4.5 Discussion

4.5.1 Evaluation on Experimental Results

The data in the table shows notable trends in the performance of our photovoltaic devices, where different configurations and treatment methods influence their efficiency and fill factor.

Integrating a CZTS layer into the device structure, either in combination with PEDOT:PSS, or as a separate layer, typically results a small gain in efficiency. For instance, the device with In/Ga/n-si/CZTS/PEDOT:PSS/Au treated with FLA at 16 J/cm² had a higher efficiency of 5.52 % than a similar device without the CZTS

Table 4.1: Photovoltaic device performance with different configurations and treatment methods.

Device Structure	**Thermal Annealing (°C)**	**FLA (J/cm^2)**	**Efficiency (%)**	**Fill Factor (FF)**
In/Ga/n-Si/PEDOT:PSS/Au	75		(4.82 ± 0.06)	(0.44 ± 0.01)
In/Ga/n-Si/PEDOT:PSS/Au		14	(5.09 ± 0.27)	(0.49 ± 0.02)
In/Ga/n-Si/PEDOT:PSS - CZTS/Au	75		(5.06 ± 0.04)	(0.44 ± 0.01)
In/Ga/n-Si/PEDOT:PSS - CZTS/Au		16	(5.11 ± 0.02)	(0.42 ± 0.01)
In/Ga/n-Si/CZTS/ PEDOT:PSS/Au	75		(4.47 ± 0.20)	(0.53 ± 0.03)
In/Ga/n-Si/CZTS/ PEDOT:PSS/Au		**16**	**(5.52 ± 0.24)**	**(0.51 ± 0.02)**
In/Ga/n-Si/CZTS/PEDOT:PSS /CZTS/PEDOT:PSS/Au		16	(3.93 ± 0.21)	(0.54 ± 0.03)

layer. Our findings indicate that CZTS, a key material in the study, significantly contributes to the overall performance of the photovoltaic device. This underscores the importance of CZTS in the field of photovoltaic devices and materials science. Interestingly, although FLA often enhances efficiency, the fill factor tends to be slightly drop in FLA-treated devices compared to those treated with thermal annealing. This phenomenon implies that there could be an acceptable balance between achieving higher efficiency and maintaining a high fill factor, potentially caused by changes in the material characteristics or layer interactions by rapid heating in FLA.

In addition, the experiment that utilized a more complex double layering of CZTS and PEDOT:PSS showed a reduction in efficiency to 3.93 % with FLA while also achieving the maximum fill factor of 0.54. This finding indicates that while the addition of several layers can enhance certain characteristics of the device, such as the fill factor, it may also complicate charge transfer or hinder light absorption efficiency, resulting in a reduction in the overall solar conversion efficiency. These findings highlight the complexities of designing photovoltaic device structures, as well as the importance of carefully balancing different layers and treatment procedures in order to obtain optimal performance.

Table 4.2: Photovoltaic device performance trends in literature.

Author	**Device Structure**	**Thermal Annealing (°C)**	**Efficiency (%)**	**Fill Factor (FF)**
Kondratenko et al. [36]	In/Ga/n-Si/PEDOT:PSS/Au	140	7	0.55
Mkawi et al. [81]	Glass/ITO/ZNO/ P3HT:PCBM:CZTS/Ag	160	3.11	0.68
Gao et al. [82]	Glass/ITO/PEDOT:PSS/ P3HT:PCBM/Al	130	2.81	0.46
Gao et al. [82]	Glass/ITO/PEDOT:PSS/Au/ P3HT:PCBM/Al	130	3.25	0.51

4.5.2 Comparative Evaluation of the Experimental Results With Literature Insights

In our investigation, we examined the performance of various PV devices from scientific literature, focusing on the impact of device structure and thermal annealing on efficiency and fill factor. However, we did not find comparable studies involving FLA.

Inspired by the In/Ga/n-Si/PEDOT:PSS/Au device structure documented in the literature [36], which demonstrated an efficiency of 7 % and a fill factor of 0.55 upon annealing at 140 °C, our research adopted a similar configuration and preparation methodology for our experiments with pure PEDOT:PSS. However, in our case, the optimal thermal annealing temperature was 75 °C. This annealing temperature change represents the specific thermal behaviors and material interactions in our PEDOT:PSS and n-Si device. Our experimental results contrast significantly from those published in the literature [34], where a similar In/Ga/n-Si/PEDOT:PSS/Au structure obtained an efficiency of 7 % and a fill factor of 0.55 after annealing at 140 °C. Our experiment, which used an annealing temperature of 75 °C, resulted in an efficiency of 4.82 ± 0.06 % and a fill factor of 0.44. The reduced efficiency in the PV device may also be affected by variations in material quality, layer thickness, and environmental conditions during testing.

The literature research [81] provides a detailed investigation into the impact of CZTS nanoparticles when combined with a P3HT:PCBM polymer blend in solar cell applications. In the referenced study, the solar cell's active layers were systematically doped with different concentrations of CZTS nanoparticles (0.2, 0.4, 0.6, 0.8 mg/mL) in a P3HT: PCBM polymer matrix. However, it caused issues with solution viscosity and agglomeration at higher concentrations, specifically above 0.8 mg/mL, affecting the homogeneity and potentially the overall performance of the active layer. Consistent with the existing literature, our experiments also encountered issues with solution agglomeration when adding a higher concentration of CZTS to

the PEDOT:PSS.

From the literature [81], the Glass/ITO/ZnO/P3HT:PCBM:CZTS/Ag structure annealed at 160 °C yielded an efficiency of 3.11 % and a fill factor of 0.68; in contrast, our study's In/Ga/n-Si/PEDOT:PSS-CZTS/Au structure, annealed at 75 °C demonstrated a higher efficiency of 5.06 % with a fill factor of 0.44.

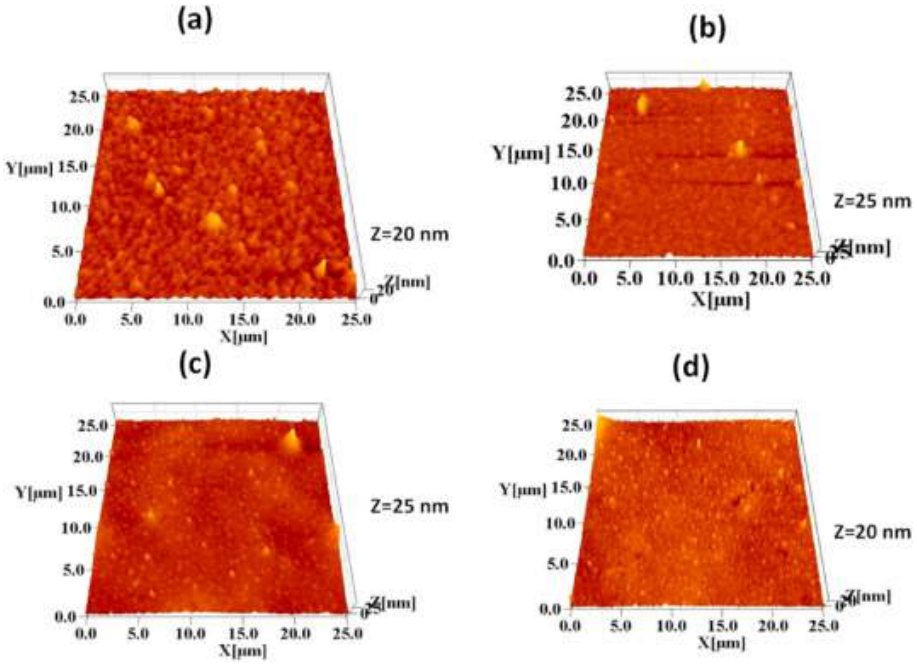

Figure 4.13: AFM images of P3HT: PCBM: CZTS NPs blended films with CZTS NPs concentrations of (a) 0.2 (b) 0.4 (c) 0.6, and (d) 0.8 mg/mL. [81]

The AFM images in **Fig. 4.13** show how the concentration of CZTS nanoparticles affects the morphology of P3HT:PCBM:CZTS films. Surface roughness decreases significantly as CZTS NP concentrations rise from 0.2 to 0.8 mg/mL, and the surface transitions from a prominent stone-like structure to a smoother, more homogeneous surface. This morphological transition, marked by reduced roughness values, suggests improved intermolecular bonding and self-assembly, enhancing the light absorption and charge transport within the film and potentially leading to better solar cell performance. [81]. Our experiments also demonstrate that incorporating CZTS into PEDOT:PSS can enhance the efficiency of solar cells, which corresponds with this finding we reviewed for inspiration. We improved on their ideas and achieved better results.

The study in the literature [82] shows how the introduction of gold (Au) nanoparticles into the PEDOT:PSS, hole transport layer of polymer solar cells, significantly affects their performance. The work demonstrates improved power conversion efficiency (PCE) for devices with integrated Au nanoparticles. Two sets of devices are compared: Glass/ITO/PEDOT:PSS/P3HT:PCBM/Al with an annealed tem-

perature of 130 °C showing an efficiency of 2.81 % and a fill factor of 0.46, and Glass/ITO/PEDOT:PSS/Au/P3HT:PCBM/Al, which showed improved efficiency at 3.25 % and a fill factor of 0.51 after annealing at the same temperature. The enhancement in PCE, is mainly as a result of the Au nanoparticles' surface plasmonic properties. These impacts resulted in increased light absorption inside the active layer and improved carrier transport efficiency within PEDOT:PSS. Inspired by these findings, our investigation also integrates gold as a top electrode in the solar cell design to exploit these advantageous properties.

5 Conclusion and Outlook

This study investigated the influence of post-treatment methods on the PV performance of Cu_2ZnSnS_4 (CZTS) QDs synthesized using a green colloidal method mixed in a PEDOT:PSS matrix. For superior efficiency enhancement, FLA outperformed the traditional thermal annealing in both pure PEDOT:PSS and CZTS-based solar cells, with the optimal CZTS to PEDOT:PSS ratio being 4 % to 96 %. This study shows that PEDOT:PSS-CZTS composites, treated with FLA at 16 J/cm^2, exhibit superior performance compared to identical composites treated with thermal annealing and pure PEDOT:PSS treated with thermal annealing and FLA. They reached a high efficiency of 5.11 % and a fill factor 0.42. These findings underscore the transformative potential of advanced post-treatment methods in enhancing the performance of environmentally friendly solar cell technologies.

Additionally, an improved efficiency was observed when employing a layered deposition technique, wherein CZTS and PEDOT:PSS were sequentially deposited— CZTS via spray coating in seven cycles and PEDOT:PSS via spin coating— rather than using the mixed deposition approach. This method led to a peak efficiency of 5.52 % with a fill factor of 0.51, further demonstrating the potential of optimized deposition strategies in enhancing solar cell performance. On the other hand, a double-layered CZTS and PEDOT:PSS solar cell configuration, treated with FLA at an energy density of 16 J/cm^2, demonstrated a reduced efficiency of 3.93 %, despite an improved fill factor of 0.54. Moreover, this setup exhibited the lowest efficiency compared to the single-layered setup and solar cells composed solely of pure PEDOT:PSS or a composite of PEDOT:PSS-CZTS.

This study's promising results on CZTS QDs embedded in a PEDOT:PSS matrix highlight future research into improving PV technologies environmentally friendly materials. Furthermore, it can be effectively integrated with innovative deposition strategies, such as layering and mixing, exploring alternative conductive polymers and substrates to enhance the commercial viability and performance of advanced solar technologies. Considering our success with the layer-by-layer PEDOT:PSS/CZTS solar cells treated at 16 J/cm^2, the effects of a 14 J/cm^2 energy density in forthcoming studies should be investigated. This particular energy density was optimal for the pure PEDOT:PSS solar cells and could potentially lead to improved efficiency and fill factor in future cell configurations.

Bibliography

[1] Balakrishna Ananthoju. "CuZnSnS nanoparticulate thin films and their solar cell characteristics". PhD thesis. Monash University, 2016.

[2] Oleksandr L. Stroyuk et al. ""Green" Aqueous Synthesis and Advanced Spectral Characterization of Size-Selected Cu2ZnSnS4 Nanocrystal Inks". In: *Scientific Reports* 8 (2018). URL: https://api.semanticscholar.org/CorpusID:52196916.

[3] F Zabihi et al. "Morphology, conductivity, and wetting characteristics of PEDOT: PSS thin films deposited by spin and spray coating". In: *Applied Surface Science* 338 (2015), pp. 163–177.

[4] César Domínguez, Ignacio Antón, and Gabriel Sala. "Solar simulator for concentrator photovoltaic systems". In: *Optics express* 16.19 (2008), pp. 14894–14901.

[5] Priscila Gonçalves Vasconcelos Sampaio and Mario Orestes Aguirre González. "Photovoltaic solar energy: Conceptual framework". In: *Renewable and sustainable energy reviews* 74 (2017), pp. 590–601.

[6] Adarsh Kumar Pandey et al. "Recent advances in solar photovoltaic systems for emerging trends and advanced applications". In: *Renewable and Sustainable Energy Reviews* 53 (2016), pp. 859–884.

[7] Umair Shahzad. "The need for renewable energy sources". In: *energy* 2 (2012), pp. 16–18.

[8] Modupeola Dada and Patricia Popoola. "Recent advances in solar photovoltaic materials and systems for energy storage applications: a review". In: *Beni-Suef University Journal of Basic and Applied Sciences* 12.1 (2023), pp. 1–15.

[9] Richard H Bube. "Materials for photovoltaics". In: *IN: Annual review of materials science. Volume 20 (A90-49626 22-23). Palo Alto* 20 (1990), pp. 19–50.

[10] J Ajayan et al. "A review of photovoltaic performance of organic/inorganic solar cells for future renewable and sustainable energy technologies". In: *Superlattices and Microstructures* 143 (2020), p. 106549.

[11] Samy Almosni et al. "Material challenges for solar cells in the twenty-first century: directions in emerging technologies". In: *Science and Technology of advanced MaTerialS* 19.1 (2018), pp. 336–369.

[12] Dongbo Wang and Yinguang Chen. "Critical review of the influences of nanoparticles on biological wastewater treatment and sludge digestion". In: *Critical reviews in biotechnology* 36.5 (2016), pp. 816–828.

[13] Clemens Burda et al. "Chemistry and properties of nanocrystals of different shapes". In: *Chemical reviews* 105.4 (2005), pp. 1025–1102.

[14] Sujung Min et al. "A review of nanomaterial based scintillators". In: *Energies* 14.22 (2021), p. 7701.

[15] Mee Rahn Kim and Dongling Ma. "Quantum-dot-based solar cells: recent advances, strategies, and challenges". In: *The journal of physical chemistry letters* 6.1 (2015), pp. 85–99.

[16] Maksym V Kovalenko. "Opportunities and challenges for quantum dot photovoltaics". In: *Nature nanotechnology* 10.12 (2015), pp. 994–997.

[17] Francesco Puoci et al. *Advanced polymers in medicine*. Springer, 2015.

[18] Jiang Li, Alayna Brieann Huckleby, and Mei Zhang. "Polymer-based thermoelectric materials: A review of power factor improving strategies". In: *Journal of Materiomics* 8.1 (2022), pp. 204–220.

[19] Pei Cheng and Xiaowei Zhan. "Stability of organic solar cells: challenges and strategies". In: *Chemical Society Reviews* 45.9 (2016), pp. 2544–2582.

[20] Tahta Amrillah. "Enhancing the value of environment-friendly CZTS compound for next generation photovoltaic device: A review". In: *Solar Energy* 263 (2023), p. 111982.

[21] Qiheng Liu et al. "Natural intermediate band in I 2-II-IV-VI4 quaternary chalcogenide semiconductors". In: *Scientific Reports* 8.1 (2018), p. 1604.

[22] M Ravindiran and C Praveenkumar. "Status review and the future prospects of CZTS based solar cell–A novel approach on the device structure and material modeling for CZTS based photovoltaic device". In: *Renewable and Sustainable Energy Reviews* 94 (2018), pp. 317–329.

[23] Balakrishna Ananthoju et al. "Cation/anion substitution in Cu2ZnSnS4 for improved photovoltaic performance". In: *Scientific reports* 6.1 (2016), p. 35369.

[24] Balakrishna Ananthoju et al. "Influence of the Cu2ZnSnS4 nanoparticles size on solar cell performance". In: *Solar energy materials and solar cells* 189 (2019), pp. 125–132.

[25] Kusum Rawat and PK Shishodia. "Thermal annealing induced modification on structural and optical properties of Cu2ZnSnS4 thin films for solar cell application". In: *Superlattices and Microstructures* 122 (2018), pp. 444–452.

[26] Yevhenii Havryliuk et al. "Influence of Thermal and Flash-Lamp Annealing on the Thermoelectrical Properties of Cu2ZnSnS4 Nanocrystals Obtained by "Green" Colloidal Synthesis". In: *Nanomaterials* 13.11 (2023), p. 1775.

[27] Kuan Sun et al. "Review on application of PEDOTs and PEDOT: PSS in energy conversion and storage devices". In: *Journal of Materials Science: Materials in Electronics* 26 (2015), pp. 4438–4462.

[28] Yan Yang, Hua Deng, and Qiang Fu. "Recent progress on PEDOT: PSS based polymer blends and composites for flexible electronics and thermoelectric devices". In: *Materials Chemistry Frontiers* 4.11 (2020), pp. 3130–3152.

[29] Granch Berhe Tseghai et al. "PEDOT: PSS-based conductive textiles and their applications". In: *Sensors* 20.7 (2020), p. 1881.

[30] Yijie Xia and Shuyang Dai. "Review on applications of PEDOTs and PEDOT: PSS in perovskite solar cells". In: *Journal of materials science: materials in electronics* 32.10 (2021), pp. 12746–12757.

[31] Vinamrita Singh and Tanuj Kumar. "Study of modified PEDOT: PSS for tuning the optical properties of its conductive thin films". In: *Journal of Science: Advanced Materials and Devices* 4.4 (2019), pp. 538–543.

[32] Katherine A Mazzio and Christine K Luscombe. "The future of organic photovoltaics". In: *Chemical Society Reviews* 44.1 (2015), pp. 78–90.

[33] Zhe Sun et al. "Performance-enhancing approaches for PEDOT: PSS-Si hybrid solar cells". In: *Angewandte Chemie International Edition* 60.10 (2021), pp. 5036–5055.

[34] Xuning Zhang et al. "Recent progress in hole-transporting layers of conventional organic solar cells with p–i–n structure". In: *Advanced Functional Materials* 32.44 (2022), p. 2205398.

[35] Chenxu Zhang et al. "Efficient planar hybrid n-Si/PEDOT: PSS solar cells with power conversion efficiency up to 13.31% achieved by controlling the SiOx interlayer". In: *Energies* 11.6 (2018), p. 1397.

[36] Serhiy Kondratenko et al. "Charge carrier transport, trapping, and recombination in PEDOT: PSS/n-Si solar cells". In: *ACS Applied Energy Materials* 2.8 (2019), pp. 5983–5991.

[37] Natsumi Ikeda et al. "Performance of Si/PEDOT: PSS hybrid solar cell controlled by PEDOT: PSS film nanostructure". In: *The Journal of Physical Chemistry C* 120.34 (2016), pp. 19043–19048.

[38] Duong Nguyen Nguyen et al. "Molecular manipulation of PEDOT: PSS for efficient hole transport by incorporation of N-doped carbon quantum dots". In: *Dyes and Pigments* 194 (2021), p. 109610.

[39] Prashant V Kamat. "Quantum dot solar cells. The next big thing in photovoltaics". In: *The journal of physical chemistry letters* 4.6 (2013), pp. 908–918.

[40] Daniel D Tune et al. "Carbon nanotube-silicon solar cells". In: *Advanced Energy Materials* 2.9 (2012), pp. 1043–1055.

[41] Werner Kern and Klaus K Schuegraf. "Deposition technologies and applications: Introduction and overview". In: *Handbook of Thin Film Deposition Processes and Techniques*. Elsevier, 2001, pp. 11–43.

[42] Ionela Andreea Neacşu et al. "Inorganic micro-and nanostructured implants for tissue engineering". In: *Nanobiomaterials in Hard Tissue Engineering*. Elsevier, 2016, pp. 271–295.

[43] David Grosso. "How to exploit the full potential of the dip-coating process to better control film formation". In: *Journal of Materials Chemistry* 21.43 (2011), pp. 17033–17038.

[44] Xuelian Wu et al. "Preparation of Bi-based photocatalysts in the form of powdered particles and thin films: a review". In: *Journal of materials chemistry A* 8.31 (2020), pp. 15302–15318.

[45] Chuantian Zuo and Liming Ding. "Drop-casting to make efficient perovskite solar cells under high humidity". In: *Angewandte Chemie* 133.20 (2021), pp. 11342–11346.

[46] Archana Kaliyaraj Selva Kumar et al. "A mini-review: How reliable is the drop casting technique?" In: *Electrochemistry Communications* 121 (2020), p. 106867. ISSN: 1388-2481. DOI: https://doi.org/10.1016/j.elecom.2020.106867. URL: https://www.sciencedirect.com/science/article/pii/S1388248120302186.

[47] Andresa Baptista et al. "Sputtering physical vapour deposition (PVD) coatings: A critical review on process improvement and market trend demands". In: *Coatings* 8.11 (2018), p. 402.

[48] Stephen Rossnagel. "Sputtering and sputter deposition". In: *Handbook of Thin Film Deposition Processes and Techniques*. Elsevier, 2001, pp. 319–348.

[49] Marianna Bellardita et al. "Preparation of catalysts and photocatalysts used for similar processes". In: *Heterogeneous Photocatalysis*. Elsevier, 2019, pp. 25–56.

[50] Dapeng Sun et al. "Thin film deposition techniques in surface engineering strategies for advanced lithium-ion batteries". In: *Coatings* 13.3 (2023), p. 505.

[51] John A Thornton. "Sputter Coating—Its Principles and Potential". In: *SAE Transactions* (1973), pp. 1787–1805.

[52] MD Tyona. "A theoritical study on spin coating technique". In: *Advances in materials Research* 2.4 (2013), p. 195.

[53] Haveen Ahmed Mustafa Mustafa and Dler Adil Jameel. "Modeling and the main stages of spin coating process: A review". In: *Journal of Applied Science and Technology Trends* 2.02 (2021), pp. 119–123.

[54] Bekir Sami Yilbas, Abdullah Al-Sharafi, and Haider Ali. *Self-cleaning of surfaces and water droplet mobility*. Elsevier, 2019.

[55] Niranjan Sahu, B Parija, and Sreeram Panigrahi. "Fundamental understanding and modeling of spin coating process: A review". In: *Indian Journal of Physics* 83.4 (2009), pp. 493–502.

[56] F Aziz and Ahmad Fauzi Ismail. "Spray coating methods for polymer solar cells fabrication: A review". In: *Materials Science in Semiconductor Processing* 39 (2015), pp. 416–425.

[57] Andrea Reale et al. "Spray Coating for Polymer Solar Cells: An Up-to-Date Overview". In: *Energy Technology* 3.4 (2015), pp. 385–406.

[58] George Makrides et al. "Temperature and thermal annealing effects on different photovoltaic technologies". In: *Renewable Energy* 43 (2012), pp. 407–417.

[59] Lars Rebohle et al. "A snapshot review on flash lamp annealing of semiconductor materials". In: *MRS Advances* 7.36 (2022), pp. 1301–1309.

[60] R.A. McMahon et al. "Flash-lamp annealing of semiconductor materials—Applications and process models". In: *Vacuum* 81.10 (2007). Proceedings of the sixth International Conference on Ion Implantation and Other Applications of Ions and Electrons (ION 2006), pp. 1301–1305. ISSN: 0042-207X. DOI: https://doi.org/10.1016/j.vacuum.2007.01.033. URL: https://www.sciencedirect.com/science/article/pii/S0042207X0700053X.

[61] Young Chai Cho and Sung Il Ahn. "Fabricating a Raman spectrometer using an optical pickup unit and pulsed power". In: *Scientific reports* 10.1 (2020), p. 11692.

[62] Paul Rostron, Safa Gaber, and Dina Gaber. "Raman spectroscopy, review". In: *laser* 21 (2016), p. 24.

[63] Abhijit Biswas, Tao Wang, and Alexandru S Biris. "Single metal nanoparticle spectroscopy: optical characterization of individual nanosystems for biomedical applications". In: *Nanoscale* 2.9 (2010), pp. 1560–1572.

[64] Mohamed Shaban et al. "Synthesis and characterization of Tin oxide thin film, effect of annealing on multilayer film". In: *J. Mod. Trends Phys. Res* 14 (2014), pp. 90–99.

[65] Sun-Young Park et al. "Spray-coated organic solar cells with large-area of 12.25 cm2". In: *Solar Energy Materials and Solar Cells* 95.3 (2011), pp. 852–855.

[66] Adamu Goje et al. "Review of flexible perovskite solar cells for indoor and outdoor applications". In: *Materials for Renewable and Sustainable Energy* 13 (Feb. 2024). DOI: 10.1007/s40243-024-00257-8.

[67] Wujun Wang and Björn Laumert. "Simulate a 'Sun' for Solar Research : A Literature Review of Solar Simulator Technology". In: 2014. URL: https://api.semanticscholar.org/CorpusID:106667773.

[68] "Upconversion mechanisms in rare-earth doped glasses to improve the efficiency of silicon solar cells". In: *Solar Energy Materials and Solar Cells* 95.7 (2011), pp. 1671–1677. ISSN: 0927-0248. DOI: https://doi.org/10.1016/j.solmat.2011.01.027.

[69] Hiroyasu Nishi et al. "Controllable electronic energy structure of size-controlled Cu 2 ZnSnS 4 nanoparticles prepared by a solution-based approach". In: *Physical Chemistry Chemical Physics* 16.2 (2014), pp. 672–675.

[70] Xiaoyan Zhang et al. "Efficient thermolysis route to monodisperse Cu2ZnSnS4 nanocrystals with controlled shape and structure". In: *Scientific reports* 4.1 (2014), p. 5086.

[71] Zhihong Gong et al. "A solvothermal route to synthesize kesterite Cu2ZnSnS4 nanocrystals for solution-processed solar cells". In: *Journal of Alloys and Compounds* 663 (Dec. 2015). DOI: 10.1016/j.jallcom.2015.12.181.

[72] SA Vanalakar et al. "Simplistic toxic to non-toxic hydrothermal route to synthesize Cu2ZnSnS4 nanoparticles for solar cell applications". In: *Solar Energy* 122 (2015), pp. 1146–1153.

[73] Samia Chamekh, N. Khemiri, and Mounir Kanzari. "Effect of annealing under different atmospheres of CZTS thin films as absorber layer for solar cell application". In: *SN Applied Sciences* 2 (Sept. 2020). DOI: 10.1007/s42452-020-03287-9.

[74] "Millisecond thermal processing using flash lamps for the advancement of thin layers and functional coatings". In: *Surface and Coatings Technology* 314 (2017). Selected papers from the Society of Vacuum Coaters 59th Annual Technical Conference, pp. 169–176. ISSN: 0257-8972. DOI: https://doi.org/10.1016/j.surfcoat.2016.08.010.

[75] Jaker Hossain et al. "State-of-the-Art of Solution-Processed Crystalline Silicon/Organic Heterojunction Solar Cells: Challenges and Future". In: May 2021, pp. 33–56. ISBN: 978-3-030-69444-9. DOI: 10.1007/978-3-030-69445-6_2.

[76] Gabriella Buscemi et al. "Chlorophylls as molecular semiconductors: introduction and state of art". In: *Advanced Materials Technologies* 7.2 (2022), p. 2100245.

[77] Boyuan Qi and Jizheng Wang. "Fill factor in organic solar cells". In: *Physical Chemistry Chemical Physics* 15.23 (2013), pp. 8972–8982.

[78] D Kumar Sharma and Ghanshyam Purohit. "Analysis of the effect of fill factor on the efficiency of solar PV system for improved design of MPPT". In: *6th world conference on photo voltaic energy conversion*. 2014.

[79] Youngkyoo Kim et al. "Effects of thickness and thermal annealing of the PEDOT: PSS layer on the performance of polymer solar cells". In: *Organic Electronics* 10.1 (2009), pp. 205–209.

[80] Yevhenii Havryliuk et al. "Raman Spectroscopy and Thermoelectric Characterization of Composite Thin Films of Cu2ZnSnS4 Nanocrystals Embedded in a Conductive Polymer PEDOT: PSS". In: *Nanomaterials* 13.1 (2022), p. 41.

[81] EM Mkawi et al. "Fabricated Cu2Zn SnS4 (CZTS) nanoparticles as an additive in P3HT: PCBM active layer for efficiency improvement of polymer solar cell". In: *Journal of Luminescence* 240 (2021), p. 118420.

[82] Hongli Gao et al. "Enhanced performance of polymer solar cells based on P3HT: PCBM via incorporating Au nanoparticles prepared by the micellar method". In: *Journal of Materials Science: Materials in Electronics* 31.13 (2020), pp. 10760–10767.

TECHNISCHE UNIVERSITÄT CHEMNITZ

Zentrales Prüfungsamt

Selbstständigkeitserklärung

Name: Shrestha Vorname: Dipiyanka geb. am: 09.03.1999 Matr.-Nr.: 671200	**Bitte beachten:** 1. Bitte binden Sie dieses Blatt am Ende Ihrer Arbeit ein.

Selbstständigkeitserklärung*

Ich erkläre gegenüber der Technischen Universität Chemnitz, dass ich die vorliegende Masterarbeit selbstständig und ohne Benutzung anderer als der angegebenen Quellen und Hilfsmittel angefertigt habe.

Die vorliegende Arbeit ist frei von Plagiaten. Alle Ausführungen, die wörtlich oder inhaltlich aus anderen Schriften entnommen sind, habe ich als solche kenntlich gemacht.

Diese Arbeit wurde in gleicher oder ähnlicher Form noch nicht als Prüfungsleistung eingereicht und ist auch noch nicht veröffentlicht.

Datum: 08.05.2024 Unterschrift: ……

* Statement of Authorship

I hereby certify to the Technische Universität Chemnitz that this thesis is all my own work and uses no external material other than that acknowledged in the text.

This work contains no plagiarism and all sentences or passages directly quoted from other people's work or including content derived from such work have been specifically credited to the authors and sources.

This paper has neither been submitted in the same or a similar form to any other examiner nor for the award of any other degree, nor has it previously been published.